Diagenetic effects on the molecular structure of biogenic silica: Implications for palaeoclimate research

Thesis submitted in accordance with the requirements of the University of Adelaide for an Honours Degree in Geology

Zoe Petrinolis

November 2016

THE UNIVERSITY of ADELAIDE

DIAGENETIC EFFECTS ON THE MOLECULAR STRUCTURE OF BIOGENIC SILICA: IMPLICATIONS FOR PALEOCLIMATE RESEARCH

RUNNING TITLE: SILICA CONDENSATION IN BIOGENIC SILICA

ABSTRACT

Biogenic silica is abundantly preserved in sediment and is found in diatoms and many higher plants. The isotopic composition ($\delta^{18}O_{silica}$) of biogenic silica is used widely in paleoclimate research to infer conditions in which the organism grew. However, previous studies show that secondary alterations within the matrix of biogenic silica complicate the structural and geochemical analysis of silica. This study investigates how the hydrated structure of silica changes at different temperature with time. A statistical model is constructed that quantifies the degree of silica hydration (Q_4/Q_3) by calibrating fourier transform infrared (FTIR) measurements against nuclear magnetic resonance. This study also conducts an investigation of various oxidisation techniques to find an optimal method to be used to remove organics within biogenic silica, although residual contamination proved challenging to remove in most cases. These contaminants many hinder the quantification of silica hydration using FTIR which is also used in the statistical modelling of Q_4/Q_3 measurements. The experimental results showed a relationship between time and the relative increase of the relative hydroxylation/dehydroxylation of biogenic silica. However, silica condensation is not a linear reaction, but reversible, potentially implying that the structure of silica readily undergoes temporary absorption/desorption on the surface of silica in the presence of water.

KEYWORDS

Biogenic silica

Phytoliths

Diatoms

Q_4/Q_3 - degree of silica hydration

FTIR

^{29}Si NMR

TABLE OF CONTENTS

LIST OF FIGURES

LIST OF TABLES

1. INTRODUCTION

Biogenic silica (BiSi) is abundantly preserved within sediment, deriving from organisms found in a variety of marine and non-marine environments, such as phytoliths in plants, diatoms and sponges (Fredlund, 1993; Webb & Longstaff, 2000; Leng & Barker, 2006; Hodsen *et al.,* 2008; Swann & Leng, 2009; Hodsen, 2016). The oxygen isotope composition ($\delta^{18}O_{silica}$) in BiSi is an important proxy to reconstruct marine and lacustrine paleoclimate records in locations where carbonates are poorly preserved (Leng & Barker, 2006; Swann & Leng, 2009). Past climate records are constructed based on the relationship between $\delta^{18}O_{silica}$ and the conditions in which the organism precipitated silica during growth (Moschen *et al.,* 2006). However, analysis of $\delta^{18}O_{silica}$ is beset by secondary alterations due to the naturally hydrous structure which is capable of binding to hydroxyls in water (Degens & Epstein, 1962; Mopper & Garlick, 1971; Labeyrie, 1972, 1974; Labeyrie & Julliet, 1982; Schmidt *et al.,* 2001). Secondary isotopic alterationS raise uncertainties in the integrity of $\delta^{18}O_{silica,}$ which may reflect the isotopic signal gained during diatom growth at surface water temperatures and also the conditions in bottom and pore waters (Matheney & Knauth, 1989; Brandriss *et al.,*1998; Schmidt *et al.,* 2001; Moschen *et al.,* 2006; Tyler *et al.,* 2008; Leng *et al.,* 2009; Dodd *et al.,* 2012). A greater understanding of the structural changes in BiSi is necessary to help refine palaeoclimate records (Swann & Leng, 2009). There are also many other advantageous applications of silica morphology in the biotechnology and pharmaceutical industries (Ding et al., 2008; Neethirajan *et al.,* 2009; Zhang *et al.,* 2012; Dolinina & Parfenyuk, 2014).

BiSi has an amorphous structure containing variations of Si–O–Si, Si–OH and Si–O bonds covalently bonded in a tetrahedron formation. The structure is represented by

$Si(OSi\equiv)_n\ (OH)_{4-n}$, where n = 0 to 4. (Knauth & Epstein, 1989; Graetsch, 1994; Brandriss *et al.*, 1998; Bertermann *et al.*, 2003; Gendron-Badou *et al.*, 2003; Perry, 2003; Leng *et al.*, 2009). Advancements in techniques including solid-state ^{29}Si Nuclear Magnetic Resonance (^{29}Si NMR) and Fourier Transform Infrared (FTIR) spectroscopy led to defining Q_n as the concentration of hydroxyls (OH) within a tetrahedral silica. Q represents the silicon atom, and *n* denotes the number of bridging oxygens bonded to silicon, where $n<4$ (Bertermann *et al.*, 2003; Gendron-Badou *et al.*, 2003; Leng *et al.*, 2009). Additionally, studies use Q_4/Q_3 ($[Si–(O–Si)_4]/[OH–Si–(O–Si)_3]$) to represent the degree of hydration within silica (Fig. 1) (Bertermann *et al.*, 2003; Gendron-Badou *et al.*, 2003; Gröger *et al.*, 2008).

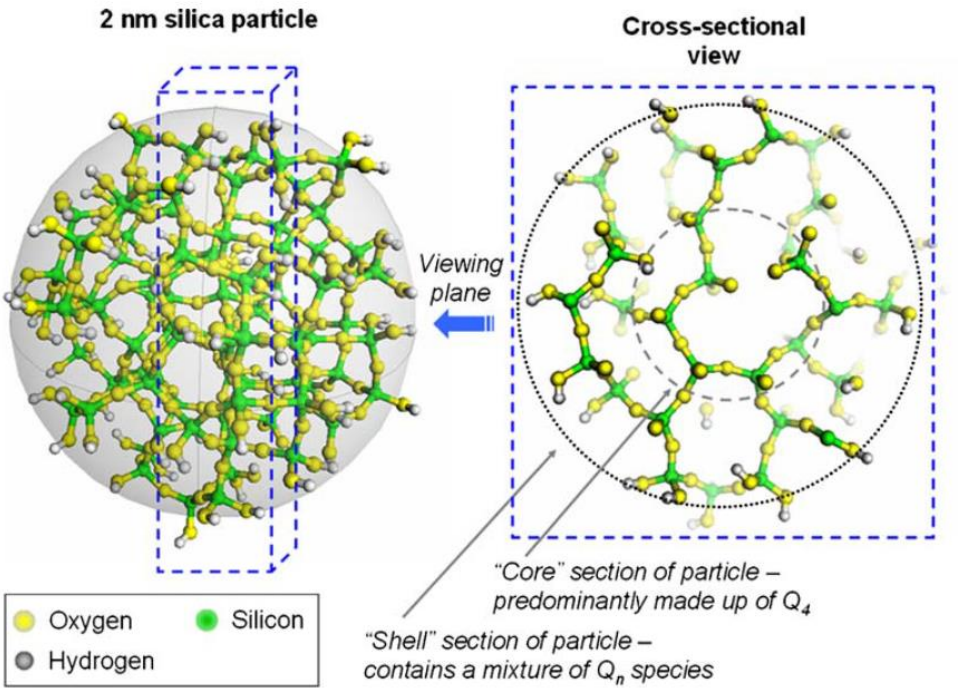

Figure 1: Representation modified from Leng el al. (2009) of diatom silica containing an outer layer with variations of hydrated silica (Q_{1-3}). The centre is usually isotopically homogeneous (crystalline) and composed of predominately Q_4.

FTIR is used to determine the vibrational frequencies of functional groups characterising specific silica species, as summarised in Table 1. FTIR also gives information about the relative strength of external and internal structural interactions of species, such as organic and inorganic material (Perry, 2003).

Table 1: A reference guide to vibrational frequencies measured by FTIR of fundamental functional groups in BiSi.

Molecular Bending/Stretching Vibrations	**Wavelength (cm^{-1})**	**Reference**
Tetrahedral SiO_4	1100, 470	(Lecomte, 1949; Schmidt *et a.l,* 2001)
Siloxane (silica backbone) Si–O–Si	800	(Lecomte, 1949; Parke, 1974: Schmidt *et al*, 2001)
Silanol (Silica network) Si–OH	945, 900	(Moenke, 1974: Schmidt *et al*, 2001)
C–OH, C–O–C, C–C Amorphous organic sequence of overlapping of organic material (polysaccharide eg. cellulose)	1200 – 1000	(Filippov, 1992; Kačuráková *et al.*, 2000)
C–H (-CH, -CH_2, -CH_3 groups) & –OH Organic matter linked to silica	1700 – 1300	(Gendron-Badou *et al.*, 2003)
C= O & H–O–H Carbonyl and water	1800 – 1650	(Gendron-Badou *et al.*, 2003)
C–H (-CH, -CH_2, -CH_3 groups) & –OH Respective overlapping of hydroxyls embedded in silica	3600 – 2900	(Moenke, 1974; Kammer *et al.*, 2010)

^{29}Si NMR spectroscopy is a more rigorous technique than FTIR because it focuses on the specific environment within the proximity of the silicon nucleus. This information quantifies the speciation in functional groups and extent of the interactions of organic and siliceous mineralisation. NMR can be used to also measure the lengths and angles of silica bonds which are used to understand the density and ordering of the silica structure (Perry, 2003).

The ability to quantify silica species can broaden the understanding of how oxygen-bearing compounds freely exchange oxygen between the hydrous-organic layer of BiSi (Fig. 1) and water. This exchangeability complicates $\delta^{18}O_{silica}$ analysis, since it is assumed the layer remains constant during and after the burial of diatoms in sediments (Schmidt *et al*., 1997; Brandriss *et al*., 1998; Moschen *et al*., 2006) or a laboratory grown culture (Tyler *et al*., 2007). This oxygen exchange is thought to occur by the following silica condensation reaction, demonstrated in Equation 1:

$$OH\text{–}Si(O\text{–}Si)_3 + OH\text{–}Si(O\text{–}Si)_3 \rightarrow Si\text{–}(O\text{–}Si)_4 + Si\text{–}(O\text{–}Si)_4 + H_2O \quad \ldots\ldots(1)$$

The condensation of silica involves two molecules of hydroxylated silica to release one molecule of water. The additional single oxygen atom derived from the hydroxyl is therefore captured within the framework of newly condensed silica molecule, thereby contaminating the $\delta^{18}O_{silica}$ signal (Labeyrie & Julliet, 1982; Schmidt *et al.,* 2001; Dodd *et al.,* 2012). During condensation, the silicon–oxygen bonds become unstable and have a lower bond energy. When water is lost (Eq. 1) it is more likely that ^{16}O is selectively released because it is isotopically lighter than ^{18}O (Schmidt *et al.,* 2001; Moschen *et al*., 2006).

Multiple studies have observed an increase of $\delta^{18}O_{silica}$ signals of living and post-mortem diatoms (Schmidt *et al.,* 2001; Moschen *et al.,* 2006; Dodd *et al.,* 2012). Schmidt *et al.* (2001) observed a 3-10 ‰ $\delta^{18}O_{silica}$ increase from fresh diatom to opal that had undergone sedimentation. Moschen *et al.* (2006) also observed an oxygen isotope composition increase of 2.5 ‰ by analysing fresh diatoms in high pH conditions. The changes of $\delta^{18}O_{silica}$ were observed as sediment settled at different water depths of 0-7 m and 16-20 m. Additionally, Dodd *et al.* (2012) observed a >7 ‰ increase in $\delta^{18}O_{silica}$ from ante- and post-mortem diatom silica from two sediment cores.

These studies used FTIR spectroscopy, unveiling an overarching patterning of increasing Q_4/Q_3 peak intensities (Fig. 2) (Schmidt *et al.* 2001; Moschen *et al.*, 2006; Dodd *et al.,* 2012). The studies also collectively observed that progressive condensation within the silica matrix of a diatom makes the frustule less susceptible to dissolution (Moschen *et al.*, 2006). However, recent studies have shown that the degree of diatom dissolution does not directly equate to the in $\delta^{18}O_{silica}$ ratios since variations of these values were found to be <1‰ (Smith *et al.,* 2016).

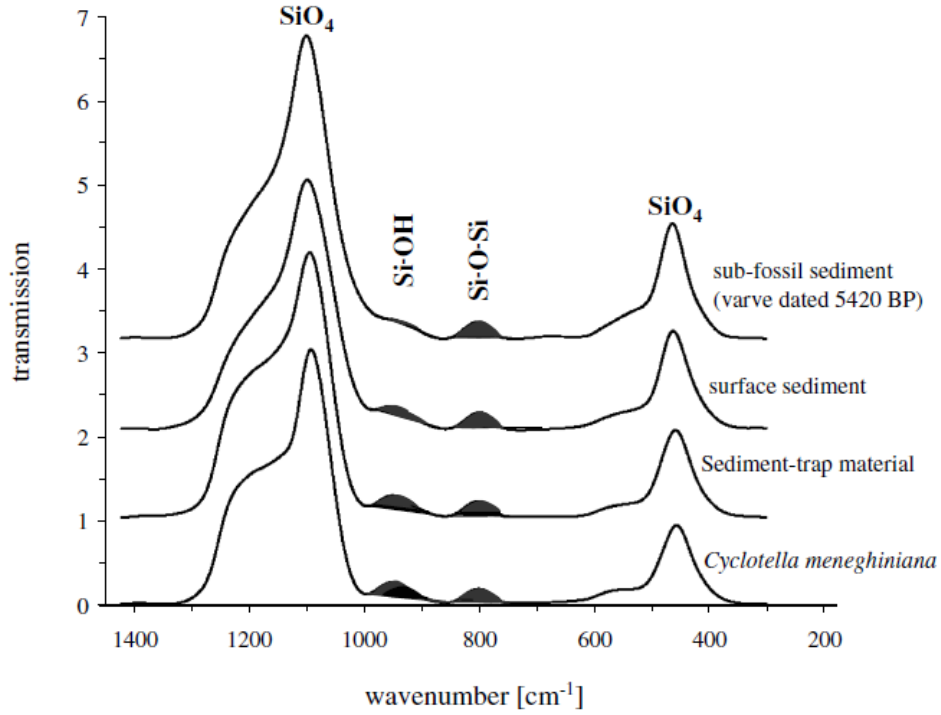

Figure 2: Modified figure from Moschen *et al.* (2006) of infrared absorption spectra of 4 different trap and sediment diatom materials. At 945 cm^{-1} the peak intensity corresponding to Si-OH weakens for sub-fossil diatoms as a result of condensation.

The studies cited above raise some important questions as to whether the changes in $\delta^{18}O_{silica}$ are caused by structural or compositional changes as Si-OH undergoes condensation. However, the full extent and rate of structural alteration within BiSi has not been addressed nor is it well understood (Dodd *et al.*, 2012). This study will take an experimental approach to explore how the hydrated structure of BiSi changes and is affected by standard laboratory practices with heating over time. The aim is to demonstrate how quickly and in what conditions the condensation reaction alters the structure of BiSi. Since FTIR and ^{29}S NMR can measure the degree of hydration, the changes in Q_4/Q_3 over time can reveal the rate of condensation. Ideally, such research would use ^{29}Si NMR as a quantitative method to measure silica condensation, but this

method is slow, expensive and needs large samples to collect results. By contrast, FTIR is readily available, fast and inexpensive, yet studies to date have only used FTIR to make quantitative inferences. This study will take a novel approach by calibrating FTIR to NMR and using both techniques to gain confidence that FTIR can obtain quantitative silica condensation measurements. It is predicted that silica hydration Q_4/Q_3 can be quantified using FTIR as indicated by a positive correlation between FTIR and NMR.

Before either BiSi Q_4/Q_3 or $\delta^{18}O_{silica}$ can be measured, the structural organic coating needs to be removed to avoid contamination (Leng & Sloane, 2008, Leng & Henderson, 2013). Tyler *et al*. (2007) tested various means of removing organic matter from silica samples, and observed minimal effects when using hydrogen peroxide and aqua regia (HNO_3 + HCl). However, that experiment was applied to Miocene age diatomite which was likely already subjected to silica condensation and diagenesis. Furthermore, although the effects upon $\delta^{18}O_{silica}$ were measured, no concurrent structural alteration was tested for. This study aims to construct an experimental method which will effectively remove organic material from BiSi with techniques which will have a minimal effect on the structure of silica.

Central to the question regarding potential silica condensation during both natural and laboratory-induced processes are the effects of temperature and time, as well as the nature of the mineral in question.

It is hypothesised that there is a positive relationship between BiSi condensation rate and temperature. In addition, less condensation is expected to occur with dense and uniform phytolith BiSi compared to the porous and high surface area of diatom samples.

2. METHODS

2.1. Collection of BiSi samples

A total of four BiSi samples were analysed in this experiment (Fig. 3). *Thalassiosira pseudonana* and *Thalassiosira weissflogii* diatom samples were sourced by Reed Mariculture Inc. provided as commercial paste for aquaculture food. A bamboo (*Dendrocalamus minor amoneus*) phytolith sample was provided by Fern Nursery Willunga. A wheat (*Triticum aestivum L. cv. Gladius)* phytolith sample was provided by Ursula Langride, University of Adelaide, School of Agriculture, Food and Wine CSIRO. Furthermore, five silica standards were analysed to undertake FTIR vs. NMR calibration. These standards had previously been analysed for NMR at the University of Oxford, as published by Chapligin *et al*. (2011). The pure silica standards did not require any sample pre-treatment before analysis.

2.2. Extraction of diatom and phytolith silica samples

Samples were digested in different oxidising reagents to remove organic material from the silica prior to structural analysis, summarised in Table 2. All samples were chemically treated via Treatment 1 before any additional treatment (2-6). Digestion of organic material was conducted by using 30% hydrogen peroxide (H_2O_2) warmed at <70˚C on a heat block (Treatments 1-6). Acid digestion was also carried out using 30 % aqua regia (1 : 3 HNO_3/HCl) (Treatments 2 and 4). Cation-exchange reaction was carried out using a 2M Barium Chloride ($BaCl_2$) solution (Treatment 3 and 4). High energy ultraviolet (UV) photo-oxidation was used to oxidise organic matter. The UV oxidiser was constructed with an arrangement of a 1.2 kW mercury vapour lamp and quartz tubes similar to that described by Skjemstad *et al*. (1994). The mercury vapour

lamp was equipped with a power supply constructed by T.A.D Electrical Industries (Adelaide, S.A.). Aliquots containing 10 mg of either bamboo or wheat samples were placed in quartz tubes, made to 10 mL with water and placed in the photo-oxidizer (Treatments 5 and 6) (Sanderman *et al.*, 2011).

Table 2: A variety of treatments used to find optimal method in removing organic material from BiSi samples.

Treatment No.	Treatment Method	Time
1	H_2O_2	24 hours @ 70˚C
2	H_2O_2 + aqua regia (1:3 HNO_3/HCl)	6 hours
3	H_2O_2 + $BaCl_2$ salt solution	6 hours
4	H_2O_2 +aqua regia (1:3 HNO_3/HCl) + $BaCl_2$ salt solution	6 hours
5*	H_2O_2 + UV photo-oxidation	2 hours
6*	H_2O_2 + UV photo-oxidation	4 hours

*Treatment No. 5 only conducted on bamboo and wheat samples

2.3. Time-temperature experimental design

Samples were stored in deionised water for periods of time (0, 3, 5, 7, 10 days) across various temperatures (4, 20, 50 80˚C) summarised in Table 3. For the first set of experiments, pH was buffered to pH 7 using TRIS (2-Amino-2-(hydroxymethyl)propane-1,3-diol). Temperature was controlled using a freezer set to 4 ˚C, laboratory room temperature of 20˚C and ovens regulated at 50˚C and 80˚C. Samples were sealed in air/water tight 2 mL HPDE centrifuge tubes.

Table 3: Experimental design of 4 samples stored in water and TRIS buffer over various time-steps at different temperatures.

	Sample Quantity	Sample Variation

Samples	4	*Thalassiosira pseudonana*, *Thalassiosira weissflogii*, bamboo and wheat
Time steps	4	0 (experimental control), 3, 5, 7, 10 days
Temperature	4	4, 20, 50 80˚C
pH	1	7**
Replicates	6	
	TOTAL sample No. : 388	

** pH was initially regulated using a TRIS buffer.

A second revised methodological experiment was conducted without the presence of a TRIS buffer. Samples were stored in water for different periods of time (0, 2, 5, 8, 10 days) across various temperatures (4, 20, 50, 80˚C) summarised in Table 4.

Table 4: Revised experimental design of 2 samples stored in water over various time-steps at different temperatures.

	Sample Quantity	**Sample Variation**
Samples	2	*Thalassiosira weissflogii*, and bamboo
Time steps	4	0 (experimental control), 3, 5, 7, 10 days
Temperature	4	4, 20, 50, 80˚C
Replicates	3	
	TOTAL sample No. : 98	

2.4. Scanning electron microscopy (SEM) of silica samples

SEM imaging was performed for visual inspection of silica to infer the level of organic contamination. Silica samples were air-dried onto specimen stubs and coated with palladium in preparation. SEM imaging was performed using a Phillips XL30 Field Emission Scanning Electron Microscope (FESEM) at 10 kV.

2.5. Elemental analysis of total carbon and nitrogen composition

A CNS-2000 analyser (LECO Corporation, St. Joseph, MI, USA) was used to measure the mass of carbon and nitrogen for all the variously treated plant samples. This procedure involves dry combustion methods with samples sizes of <500 mg which were added to the nickel-lined LECO boat (Sanderman et al., 2011).

2.6. Fourier transform infrared (FTIR) analysis

Mid - Infrared spectra were acquired for all samples in this study using a Nicolet 6700 FTIR spectrometer (Thermo Fisher Scientific Inc., Waltham, MA, USA) fitted with a KBr beam-splitter, a DTGS detector and an Auto Diff-Automated diffuse reflectance accessory (Pike Technologies, Madison, WI, USA). Spectra were acquired over 8000-400 cm^{-1} at 8 cm^{-1} resolution. A silicon carbide disk was used to collect a background signal intensity prior to analysis of samples. Samples (60 mg) were placed in a silicon cell holder and scanned 60 times to produce reflectance spectra which were converted to absorbance spectra using Omnic software (Version 8.0; Thermo Fisher Scientific Inc.) (Sanderman *et al.,* 2011).

2.7. Solid-state ^{13}C Nuclear Magnetic Resonance (NMR) analysis

^{13}C NMR spectroscopy was used to determine the relative abundance of organic molecules (>50 µm) for samples treated with H_2O_2 and photo-oxidation using a Bruker 200 MHz AVANCE spectrometer (Bruker Corporation, Billerica, MA,USA). See Sanderman *et al.* (2011) for full sample preparation method.

2.8. Integral area peak analysis

The FTIR spectra of bamboo and diatom silica samples were truncated according to area occupied by peaks in spectra representing Q_4 and Q_3 silica (Table 5).

Table 5 : FTIR wavelength range of diatom and bamboo spectra used in integral area analysis of Q_4 and Q_3.

Sample Type	**Q_3 Wavelength Range**	**Q_4 Wavelength Range**
	Peak centre : 945 cm^{-1} (Si – OH)	**Peak centre: 800 cm^{-1} (O – Si – O)**
Bamboo phytolith	887 - 914	779 - 856
***Thalassiosira weissflogii* diatom**	902 - 995	779 - 856

The spectral peaks were quantified using a method adapted from Bertermann *et al.* (2003), Gendron-Badou *et al.* (2003) and Gröger *et al*. (2008). However, Q_4 and Q_3 peak areas were calculated using FTIR spectra whereas other studies have used ^{29}Si NMR spectra to calculate Q_n values.

The upper and lower sum of the peak area was calculated and averaged to obtain the integral area using MATLAB software (Version 7.10.0. Natick, Massachusetts: The MathWorks Inc., 2010). This method was applied based on the idea illustrated in Fig. 2 where spectra are qualitatively used to show a decrease in hydrated silica peaks in FTIR (Moschen *et al.,* 2006).

2.9. Statistical Analysis

The acquired FTIR spectra were condensed to 6000-700 cm^{-1} and baseline-corrected before principle component analysis (PCA) and partial least-squared regression (PLSR) analysis were conducted. All spectral PCA and PLSR analysis was conducted using Unscrambler 10.2 software (CAMO Software AS, Olso, Norway). PCA was used on the spectra of averaged experimental replicates to identify any trends in similarity of spectra.

The PLSR statistical approach was used to calibrate FTIR spectra against NMR inferred silica Q_4/Q_3. to develop a predictive model that could be applied to all subsequent FTIR analyses. The PLSR calibration model calculated a relationship between two data matrices of published silica FTIR and NMR standards (Chapligin *et al.*,2011). This regression technique involves using a linear multivariable model that determines specific correlations within the structure of FTIR and NMR datasets (Wold *et al.*, 2001). Models were based on the wavelength range between 6000 -700 cm^{-1} and Q_4/Q_3 values were square-root transformed for numerical analysis. An initial independent calibration of the FTIR and NMR standards was conducted to obtain an external validation resulting in a reference model. The independent calibration was further verified by the application of reference sqrt_NMR against sqrt_FTIR, followed by a cross-validation of

each data point in the data set. This calibrated regression was used to evaluate the internal model performance.

The performance of model's predictability was determined by calculating the coefficient R^2 for calibrated regression. R^2 ranges between ≤ 0 and ≥ 1. The closer proximity the value is to 1, the better fit the measured values are to the regression line. The accuracy of the calibration was determined by calculating the root-mean-square error (RMSE).

3. RESULTS

3.1. Pre-treated bamboo and diatom SEM images

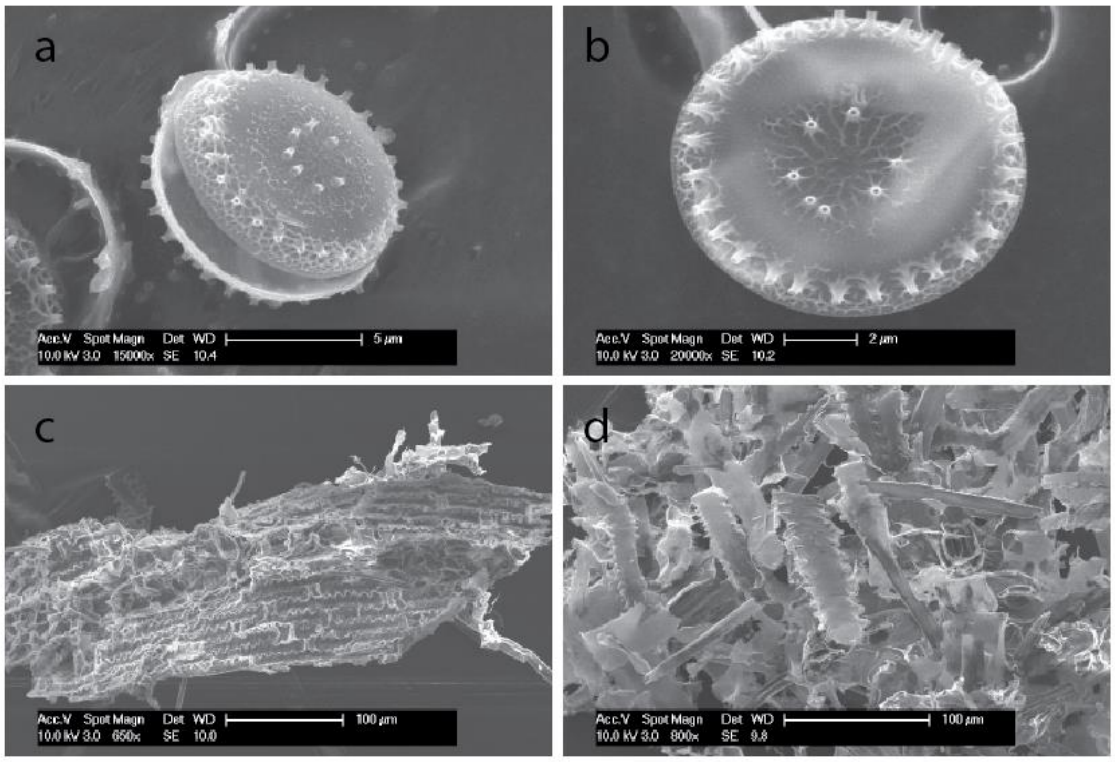

Figure 3 : Scanning election microscope (SEM) images of BiSi treated with aqua regia (1:3 HNO_3/HCl) and H_2O_2. 5a *Thalassiosira pseudonana* diatom capsule end member, external view. 5b *Thalassiosira weisflogi* diatom capsule end member, external view. 5c *Dendrocalamus mino amoneus* bamboo leaf epidermis. 5d *Triticum aestivum L. cv. Gladius* wheat leaf epidermis.

SEM images of diatoms treated using aqua regia (1:3 HNO_3/HCl) and H_2O_2 chemical reagents exhibit similar structural features (Fig. 3a,3b), such as intricate micro-porous patterned silica cell wall and small amounts of organic material. For bamboo and wheat samples, SEM analyses revealed that the treatment had left the silica with a uniform structure containing a mixture of organic material but lacking micro-morphological features (Fig. 3c, 3d).

3.2. Calibration of FTIR spectra for quantification of Q_4/Q_3

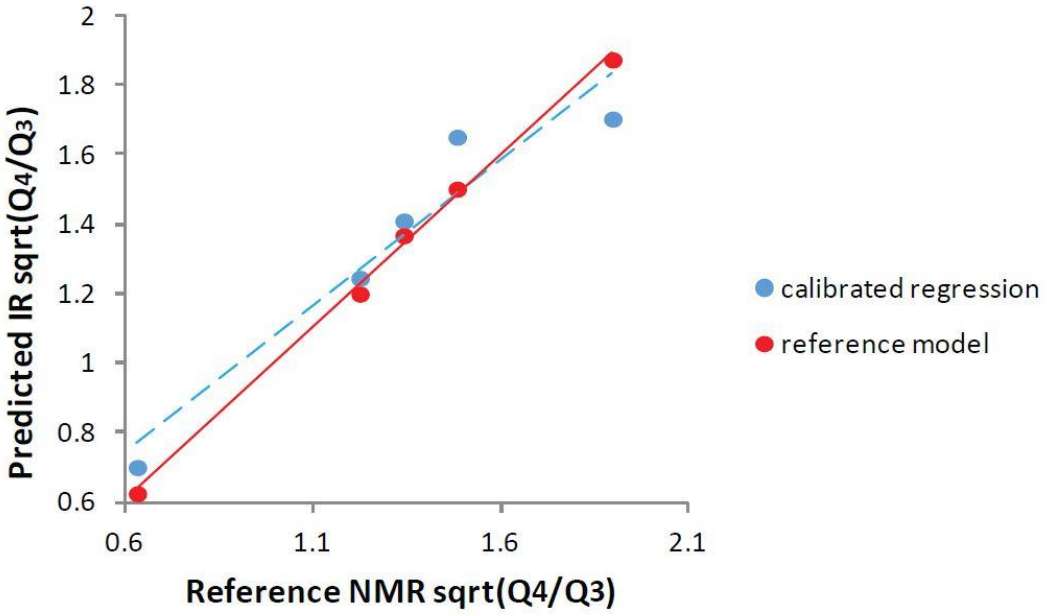

Figure 4 : Measured reference NMR vs. predicted FTIR Q_4/Q_3 values of phytolith and diatom samples (Chapligin et al. 2011). The red line represents the reference model which contains externally validated results. The blue line represents the calibrated regression which contains cross-validated results.

The calibration model for sqrt_FTIR and sqrt_NMR resulted in $R^2 = 0.94$ and RMSE = 0.12 (Fig. 4). There is a strong cross-validation between the resulting calibrated PLSR and FTIR spectral information.

3.3. Performance and effects of organic removal pre-treatments

3.3.1. ELEMENTAL ANALYSIS

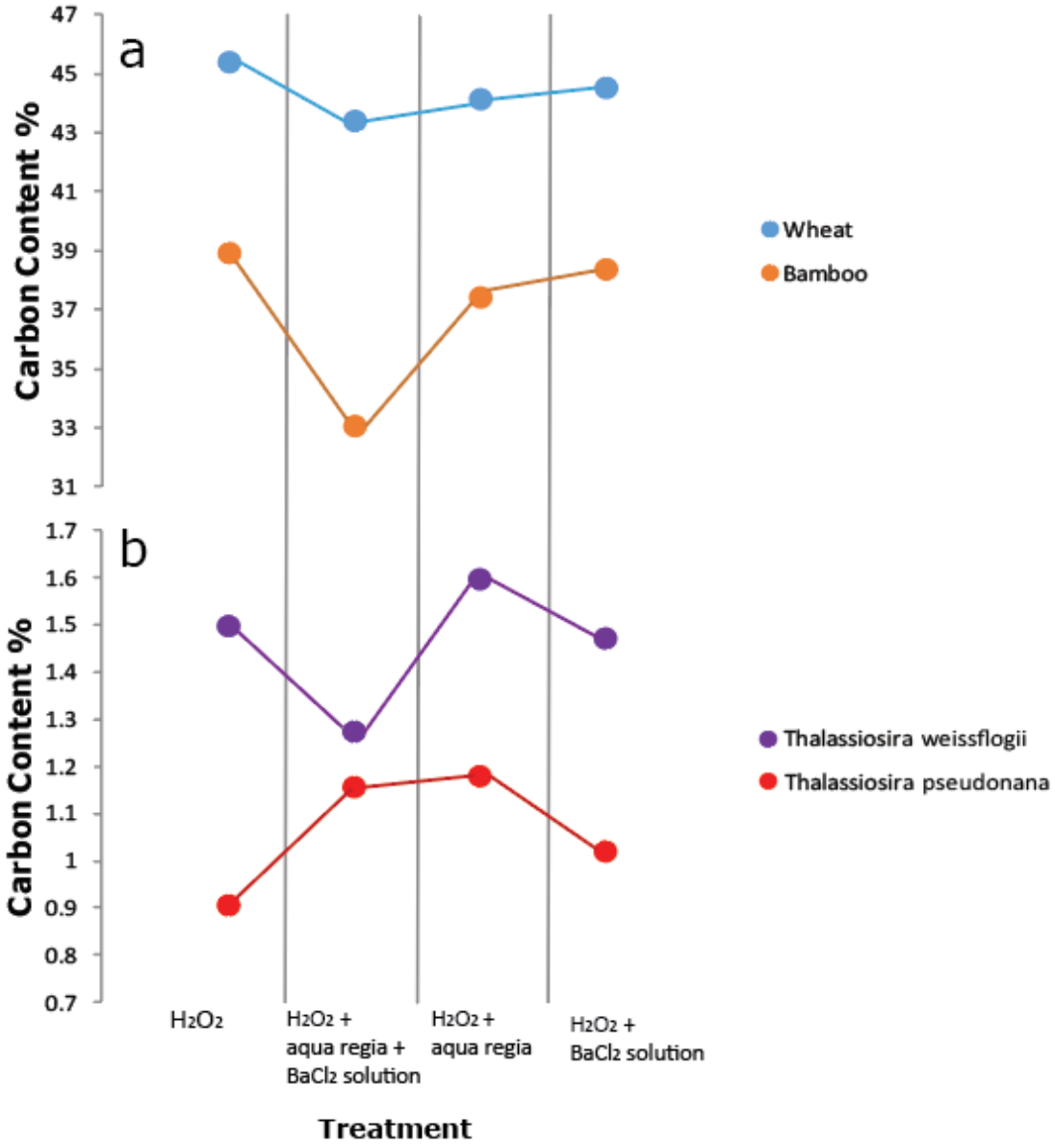

Figure 5 : Carbon content (%) of (a) leaf and (b) diatom material treated with various treatments. Blue line represents wheat sample. Orange line represents bamboo sample. Purple line represents *Thalassiosira weissflogi* sample. Red line represents *Thalassiosira Pseudonana* sample.

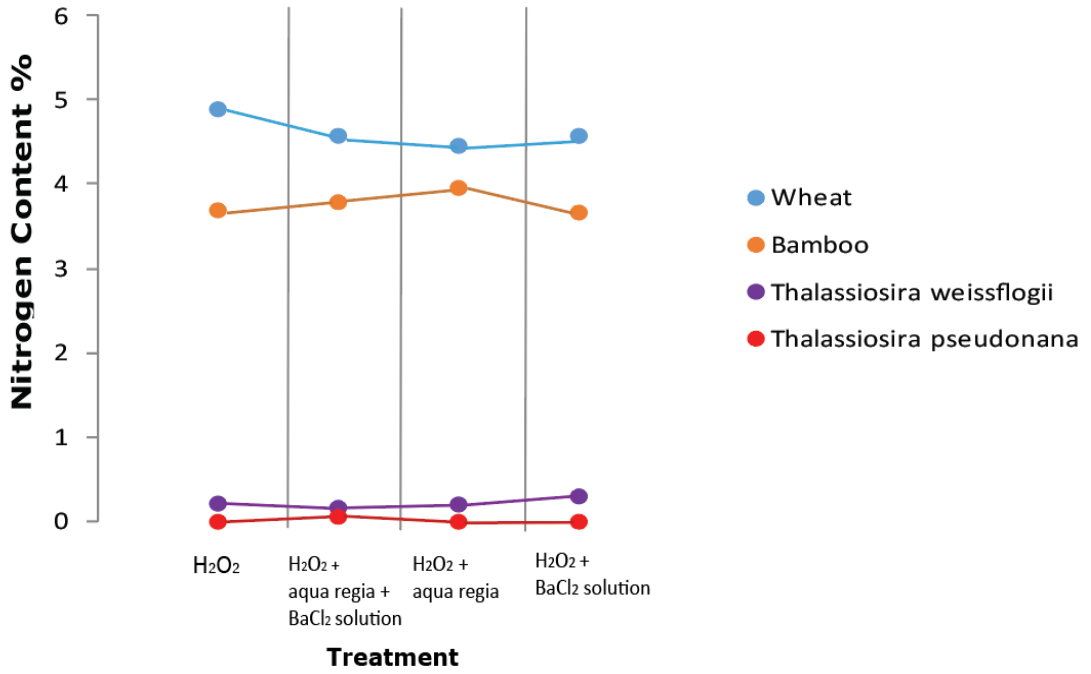

Figure 6 : Nitrogen content (%) of leaf and diatom material treated with various treatments. Blue line represents wheat sample. Orange line represents bamboo sample. Purple line represents *Thalassiosira weissflogi* sample. Red line represents *Thalassiosira Pseudonana* sample.

Despite rigorous chemical oxidation, all treated phytolith samples contained large residual quantities of carbon (~40%) and nitrogen (~4%), indicative of organic material remaining in samples (Fig. 5a, 6). The wheat samples contained a higher amount of organics than all other extracted silica samples. The treatments appear to have digested most of the organic contaminants (~1.5% residual carbon) in the diatom samples which contain the least amount organic material (Fig. 5b, 6).

As the organic removal techniques becomes more aggressive and prolonged, the concentration of residual C and N declined (Fig. 5, 6). The organic content decreases in phytolith samples with progressive treatment, however, it increases in some diatom samples albeit within the likely analytical uncertainty. There was not a large difference in the amount of organic matter removed between the different treatments.

3.3.2. ^{13}C NMR SPECTROSCOPY ANALYSIS

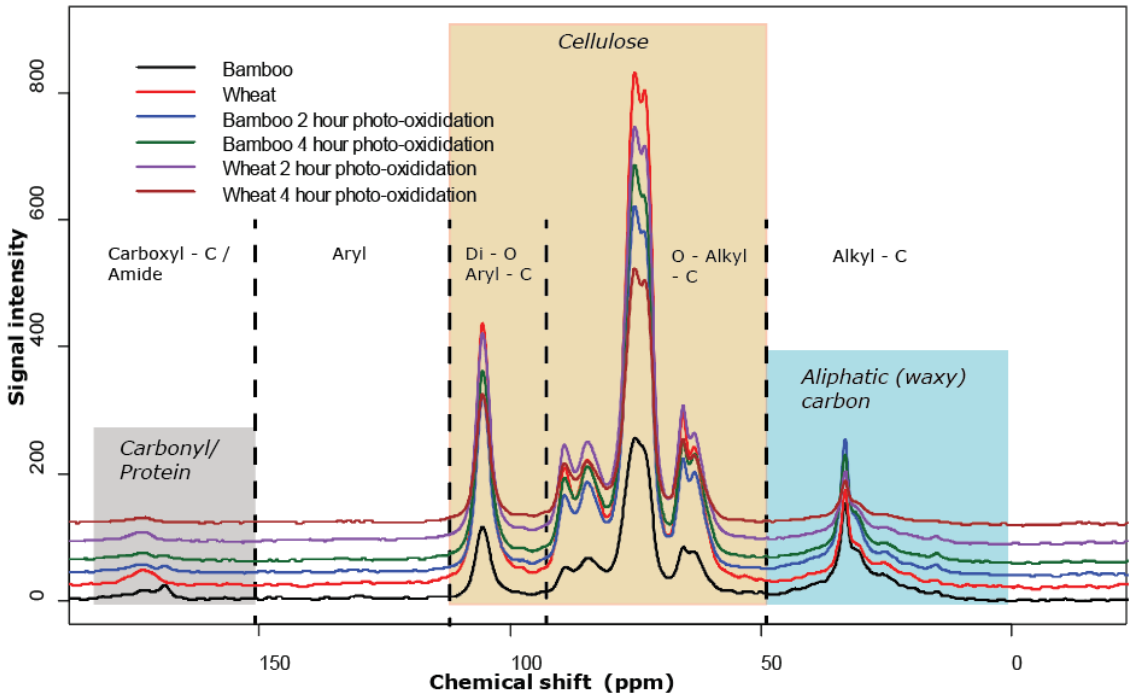

Figure 7 : Solid-state ^{13}C NMR spectra of bamboo and wheat samples treated with H_2O_2, H_2O_2 and 2 or 4 hours of photo-oxidation. The chemical shift regions of organic abundances are: 0-50 ppm (Alkyl-C), 50-90 ppm (O-Alkyl-C), 90-110 ppm (Di-O-alkyl-C), 110-165 ppm (Aryl), 165-190 ppm (Carboxyl - C/Amide/Ketone). All absorbance baselines fit the y-axis and arranged for NMR spectra comparisons between samples.

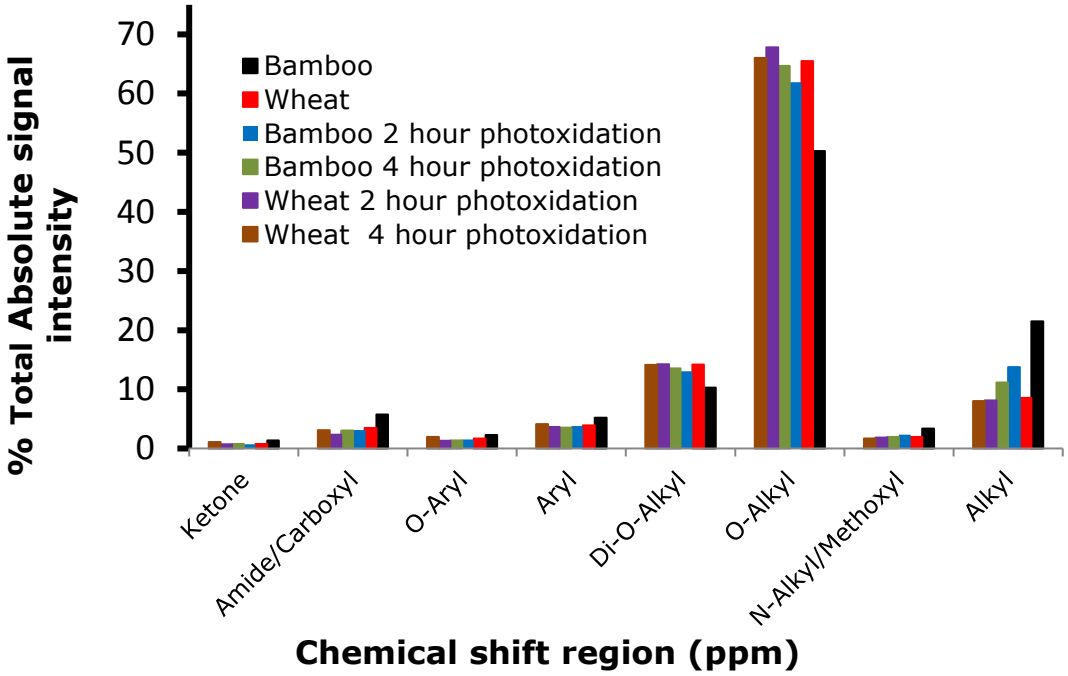

Figure 8 : Absolute % ^{13}C NMR spectral signal intensity of carbon functional groups within bamboo and wheat samples treated with H_2O_2, H_2O_2 and 2 or 4 hours of photo-oxidation.

^{13}C NMR spectroscopy unveiled 4 main resonance peaks at 40, 70, 105 and 170 ppm representing carbon functional groups which make up the majority of organic contaminants in wheat and bamboo (Fig. 7). The majority of organic material in the phytolith samples is composed of cellulose (~75%). However, bamboo treated with H_2O_2 is differentiated from the other samples yielding ~50% cellulose composition. Bamboo also exhibits the most waxy carbon (~20%), in comparison to all the other samples, and this makes up the rest of the organic material in the sample (Fig. 8). The variability of organic material content with progressive treatment is small with bamboo as the exception.

3.3.3. FTIR ANALYSIS

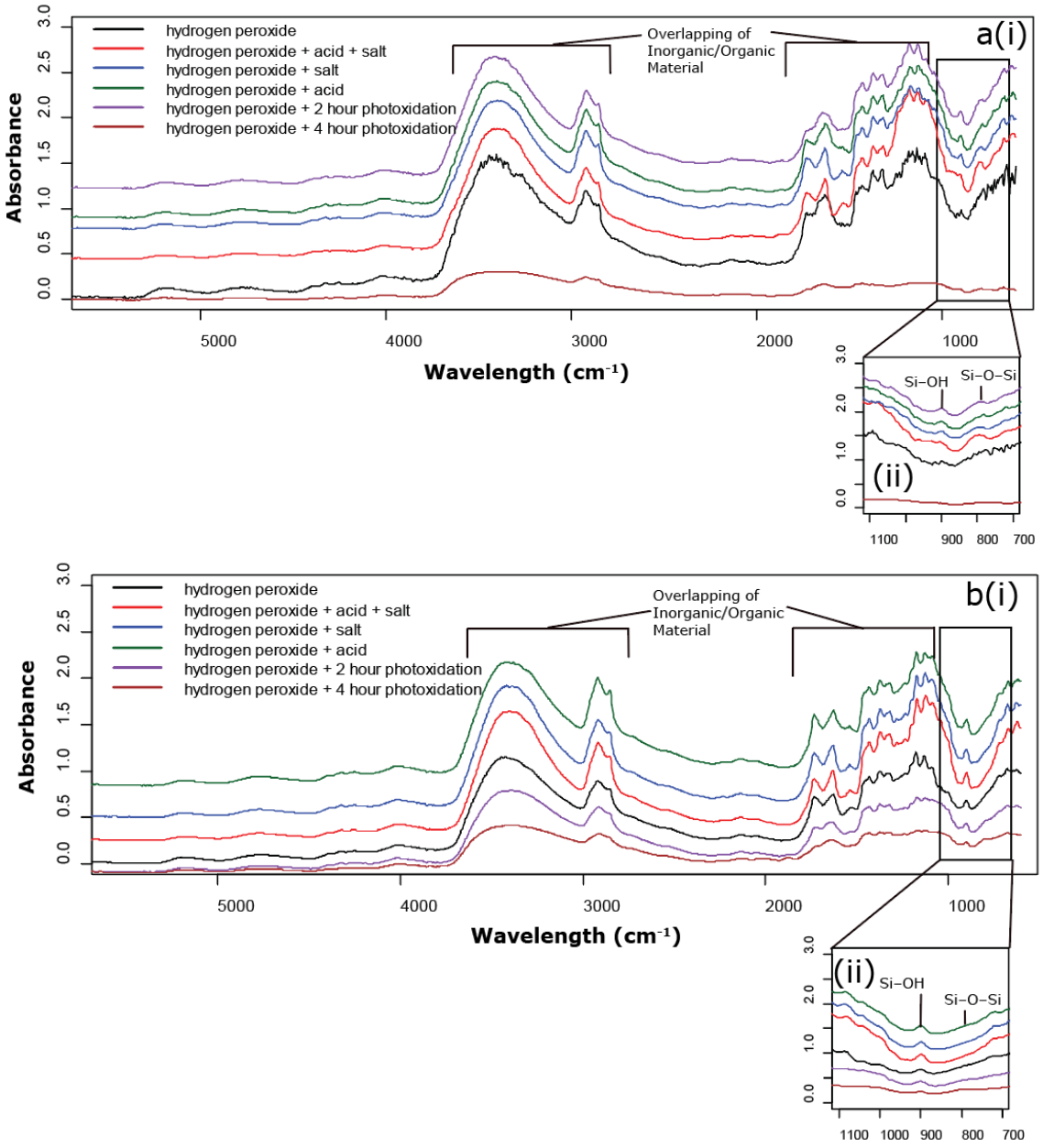

Figure 9 : FTIR spectra of (a) bamboo and (b) wheat samples treated with various treatments. Spectrum (i) has wavelength 6000-700cm^{-1} and (ii) is a magnification of the spectra wavelength between 1100-700 cm^{-1}. The multiple coloured lines represents a variety in the treatment (Black: H_2O_2, Red: H_2O_2/aqua regia/$BaCl_2$ solution, Blue: H_2O_2 /$BaCl_2$ solution, Green: H_2O_2/aqua regia, Purple: H_2O_2/ 2 hour photo-oxidation, Brown: H_2O_2/ 4 hour photo-oxidation. All absorbance baselines fit the y-axis and arranged for NMR spectra comparisons between samples.

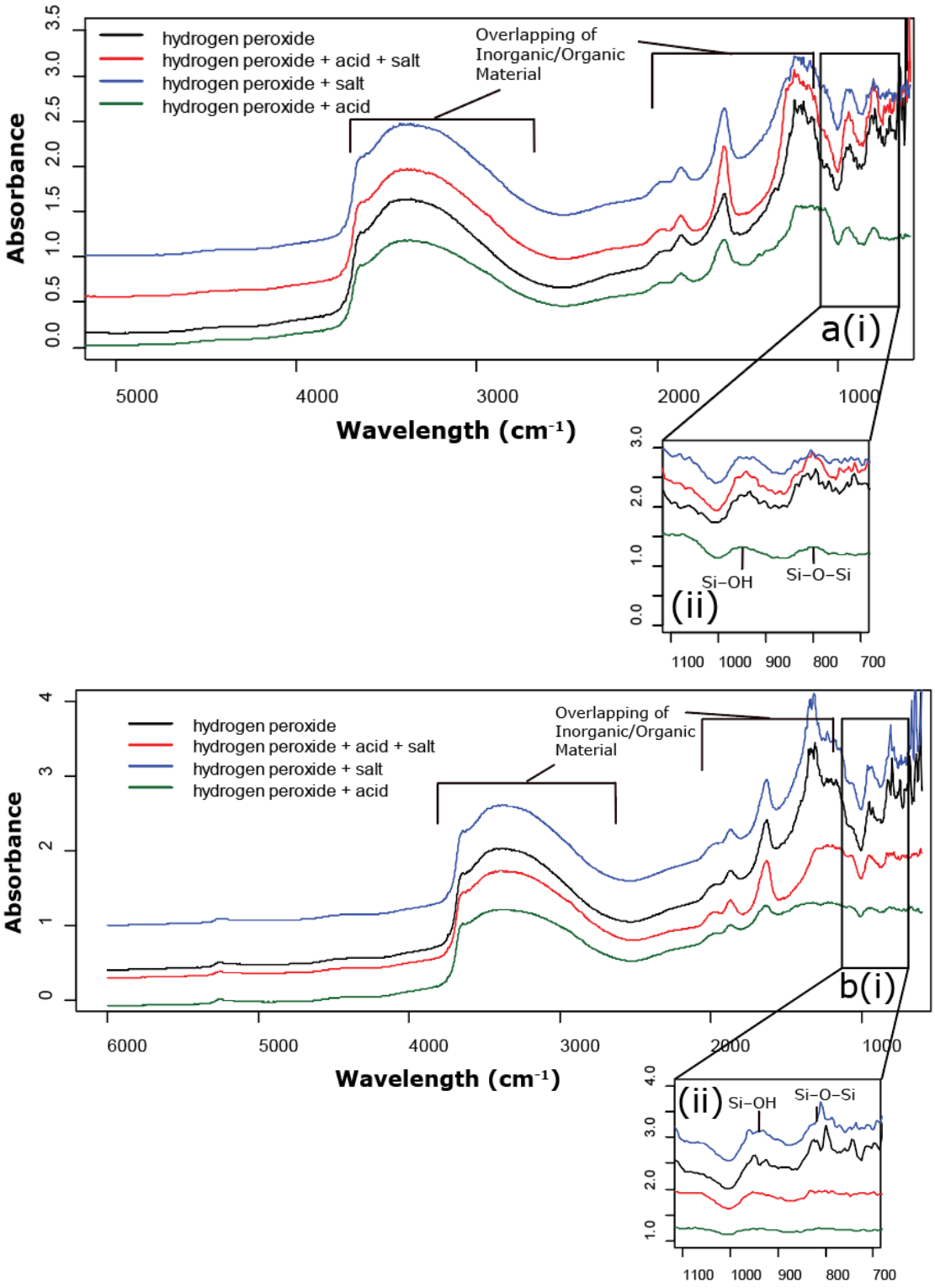

Figure 10 : FTIR spectra of (a) *Thalassiosira weissflogi* and (b) *Thalassiosira Pseudonana* diatom samples treated with various treatments. Spectrum (i) has wavelength 6000-700cm^{-1} and (ii) is a magnification of the spectra wavelength between 1100-700 cm^{-1}. The multiple coloured lines represents a variety in the treatment (Black: H_2O_2, Red: H_2O_2/aqua regia/$BaCl_2$ solution, Blue: H_2O_2 /$BaCl_2$ solution, Green: H_2O_2/aqua regia). All absorbance baselines fit the y-axis and arranged for NMR spectra comparisons between samples.

FTIR spectra show a smoothing in spectral peaks with progressive organic removal treatment to silica samples (Fig. 8, 9). The H_2O_2 treatment acquires spectra with the most additional contamination peaks, and the spectra treated with H_2O_2 and $BaCl_2$ solution remains consistently unchanged. All other treatments removed the excessively variable peaks attributed to additional molecules. Bamboo and wheat samples treated with photo-oxidation obtained spectra with extremely smooth peaks. After 4 hours of photo-oxidation the peaks related to Si-O-Si and Si-OH completely disappeared (Fig. a(ii), b(ii)).

3.4. Effects and change of structural silica with heating

The initial experiment to test the effects of temperature and time on the silica structure resulted in widespread contamination dominated by the effects of residual TRIS buffer. The contamination overlapped all additional FTIR spectral information of diatom and phytolith samples. A second experiment was therefore conducted without TRIS and using only bamboo phytolith and *Thalassiosira weissflogi* diatom samples.

3.4.1. VISUAL INSPECTION OF FTIR SPECTRA

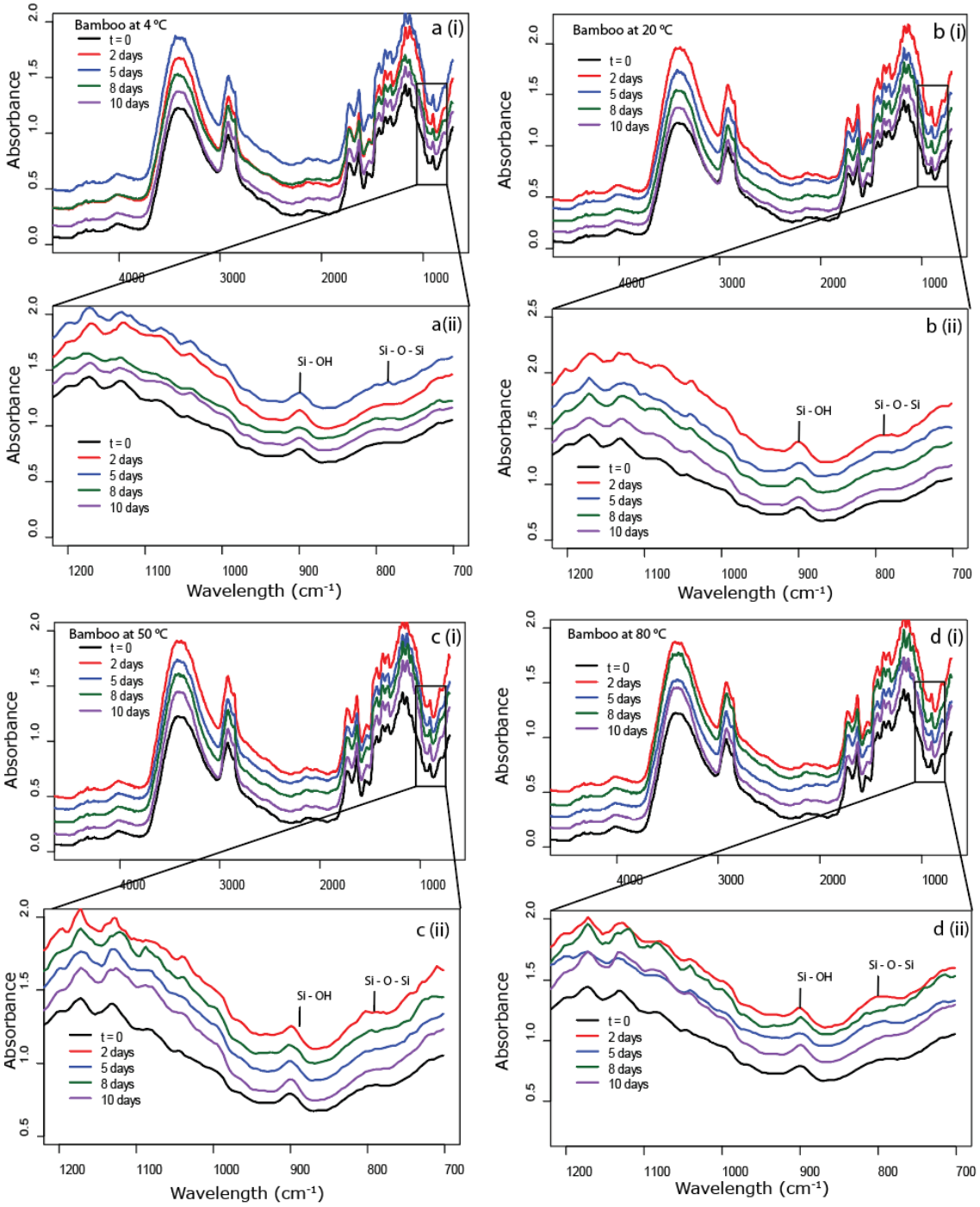

Figure 11: A comparison FTIR spectra of bamboo treated with H_2O_2 and aqua regia at experimental conditions at (a) 4˚C (b) 20˚C (c) 50˚C (d) 80˚C. Spectra (i) has wavelength 5000-700cm^{-1} and (ii) is a magnification of the spectra wavelength between 1200-700 cm^{-1}. Multiple coloured lines represents a variation of time (Black: t = 0, Red: 2 days, Blue: 5 days Green: 8 days, Purple: 10 days). All absorbance baselines fit the y-axis and arranged for NMR spectra comparisons between samples.

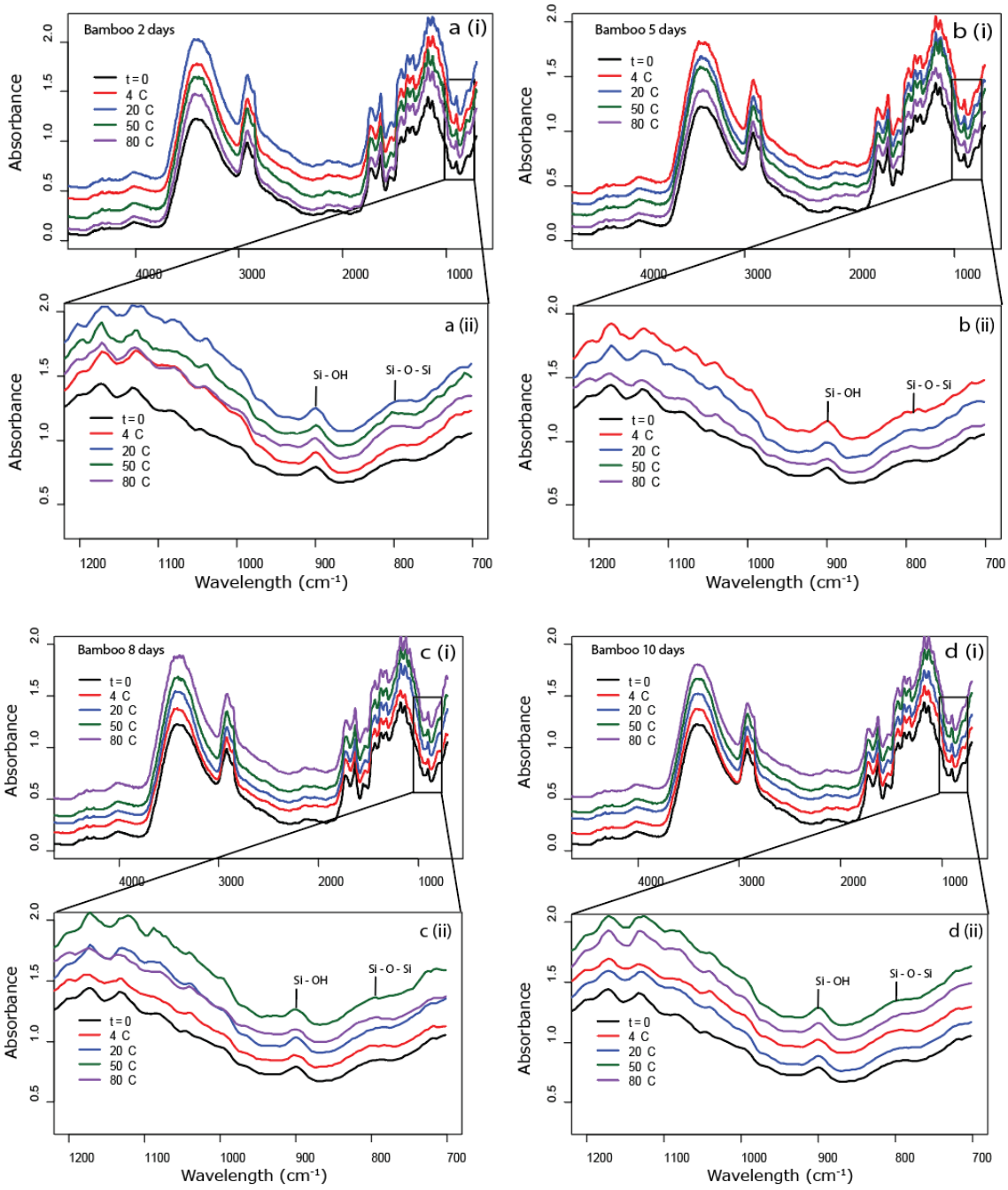

Figure 12: A comparison FTIR spectra of bamboo treated with H_2O_2 and aqua regia at various times of (a) 2 days (b) 5 days (c) 8 days (d) 10 days. Spectra (i) has wavelength 5000-700cm^{-1} and (ii) is a magnification of the spectra wavelength between 1200-700 cm^{-1}. Multiple coloured lines represents a variation in temperature (Black: t = 0, Red: 4˚C, Blue: 20˚C Green: 50˚C, Purple: 80˚C). All absorbance baselines fit the y-axis and arranged for NMR spectra comparisons between samples.

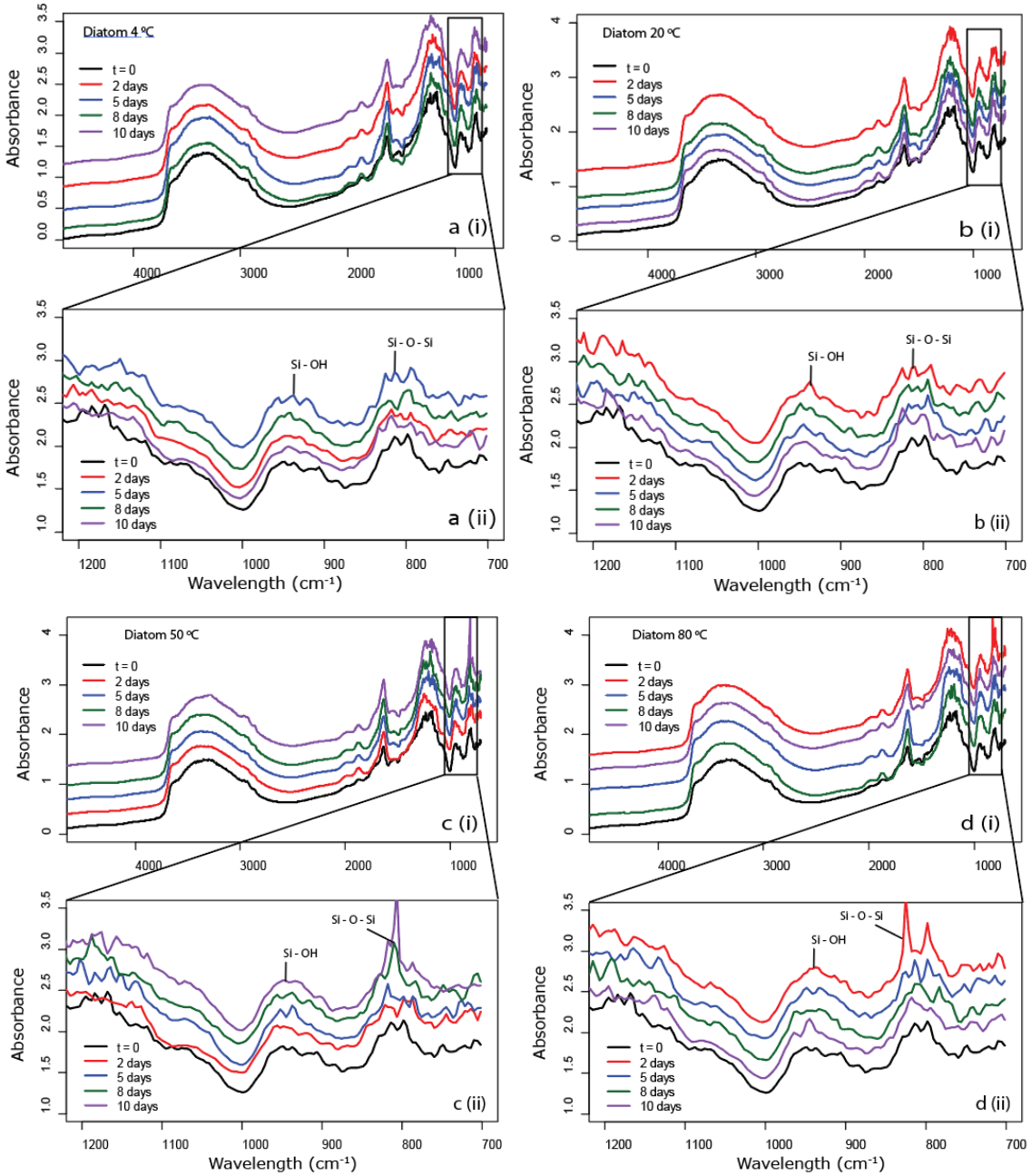

Figure 13 : A comparison FTIR spectra of *Thalassiosira weissflogi* diatoms treated with H_2O_2 and aqua regia at experimental conditions at (a) 4˚C (b) 20˚C (c) 50˚C (d) 80˚C. Spectra (i) has wavelength 5000-700cm^{-1} and (ii) is a magnification of the spectra wavelength between 1200-700 cm^{-1}. Multiple coloured lines represents a variation of time (Black: t = 0, Red: 2 days, Blue: 5 days Green: 8 days, Purple: 10 days). All absorbance baselines fit the y-axis and arranged for NMR spectra comparisons between samples

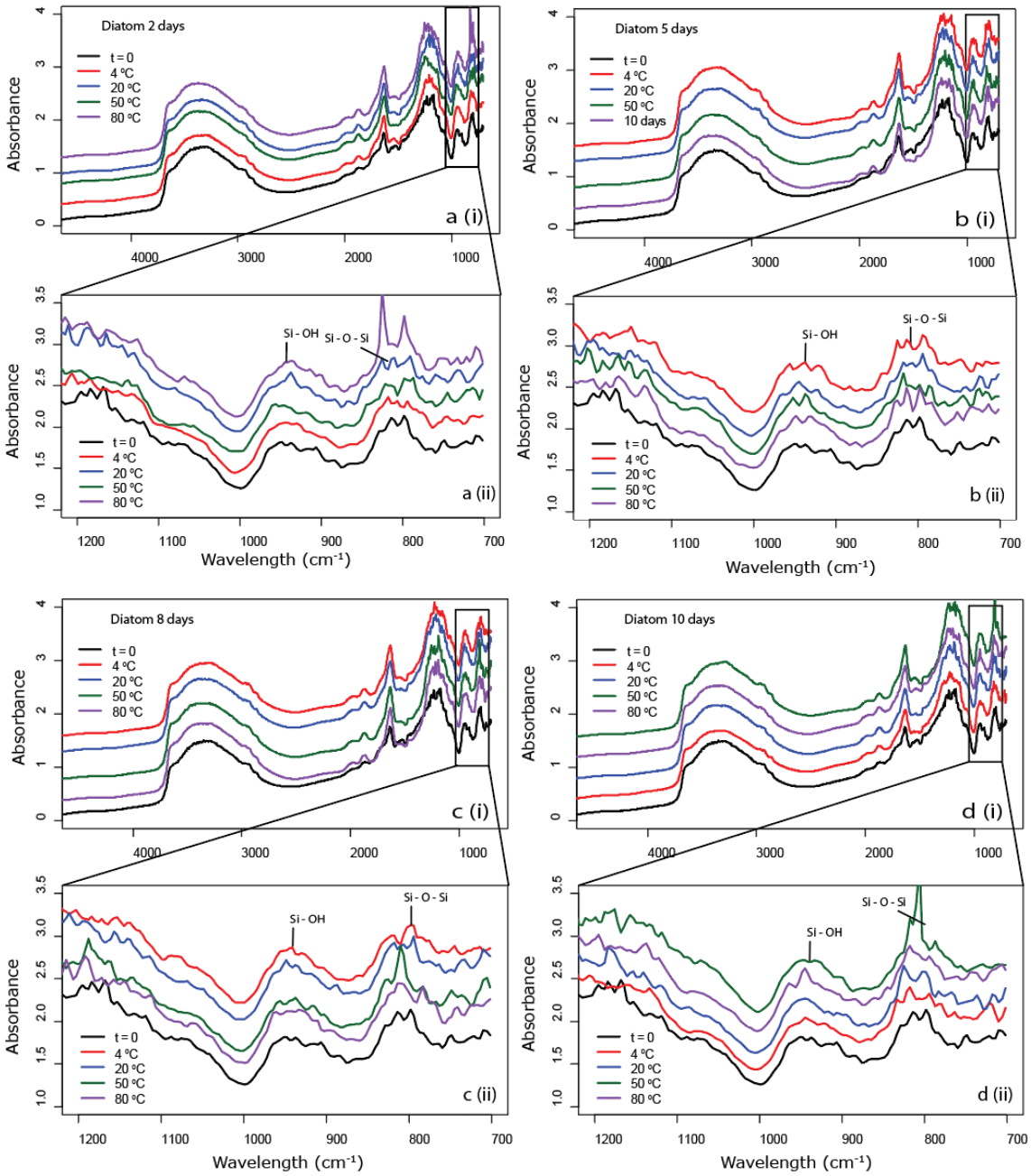

Figure 14: A comparison FTIR spectra of *Thalassiosira weissflogi* diatom treated with H_2O_2 and aqua regia at various times of (a) 2 days (b) 5 days (c) 8 days (d) 10 days. Spectra (i) has wavelength 5000-700cm^{-1} and (ii) is a magnification of the spectra wavelength between 1200-700 cm^{-1}. Multiple coloured lines represents a variation in temperature(Black: t = 0, Red: 4˚C, Blue: 20˚C Green: 50˚C, Purple: 80˚C). All absorbance baselines fit the y-axis and arranged for NMR spectra comparisons between samples.

From the visual examination of the FTIR spectra, the effects of time and temperature upon the degree of silica hydration are not immediately obvious.

The FTIR spectra peaks related to Si–OH and Si–O–Si are more pronounced for bamboo (Fig. 11,12) than for *Thalassiosira weissflogi* (Fig. 13,14) . This contrasts with the elemental analysis, that indicates that organic contamination is greater in the bamboo sample.

3.4.2. PCA ANALYSIS OF TIME-TEMPERATURE

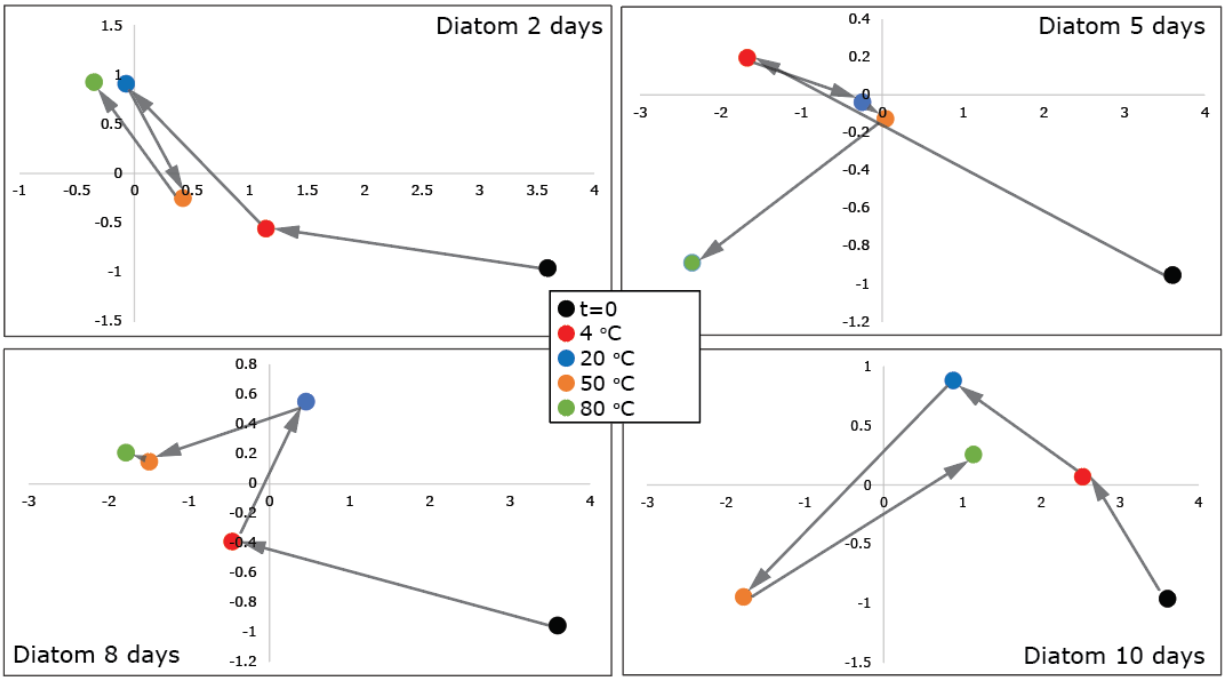

Figure 15 : A comparison Principle component analysis (PCA) plots bamboo samples cleaned with H_2O_2 and aqua regia at various times of (a) 2 days (b) 5 days (c) 8 days (d) 10 days. Multi-coloured dots represent (Black: t = 0, Red: 4˚C, Blue: 20˚C Orange: 50˚C, Green: 80˚C).

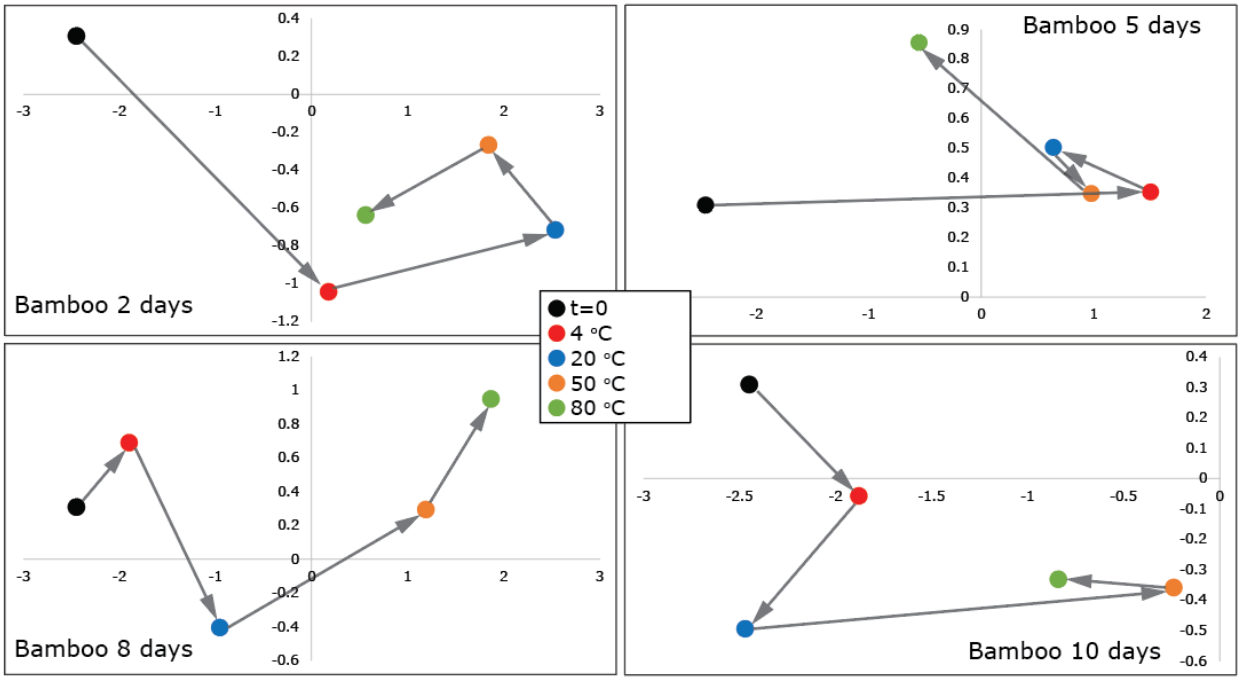

Figure 16 : A comparison Principle component analysis (PCA) plots *Thalassiosira weissflogi* diatom samples cleaned with H_2O_2 and aqua regia at various times of (a) 2 days (b) 5 days (c) 8 days (d) 10 days. Multi-coloured dots represent (Black: t = 0, Red: 4˚C, Blue: 20˚C Orange: 50˚C, Green: 80˚C).

There is no discernible trend in the PCA plots, with the exception that the largest separation in both samples exists in samples at day 2 and 5 with temperature points between t=0-4˚C and 4-20˚C (Fig. 15, 16). The other temperature points cluster closer together with even larger distances from t=0.

3.4.3. QUANTITATIVE ASSESSMENT OF SILICA HYDRATION CHANGE

Table 6 : Integral areas of Q_3, Q_4 and Q_4/Q_3 ratios calculated from the quantitative FTIR spectra and predicted Q_4/Q_3 ratios calculated by PLSR of bamboo phytolith samples cleaned with H_2O_2 and aqua regia and treated with various temperature and time conditions.

Bamboo phytolith		**Integral Area of Q_4/Q_3 in FTIR Spectra**			
Temperature (˚C)	Time (days)	Q_3 Peak centre : 945 cm^{-1} (Si – OH)	Q_4 Peak centre: 800 cm^{-1} (O – Si – O)	Q_4/Q_3 (O – Si – O/ Si –OH)	**Predicted Q_4/Q_3** (PLSR)
0	0	1.1	7.4	6.67	2.63
4	2	1.3 ± 0.12	8.7 ± 0.52	6.89 ± 0.71	2.51 ± 0.021
20	2	1.4 ± 0.18	9.9 ± 0.63	6.85 ± 0.45	2.31 ± 0.074
50	2	1.3 ± 0.041	11 ± 1.4	8.11 ± 1.3	2.29 ± 0.051
80	2	1.4 ± 0.36	11 ± 2.5	7.78 ± 0.53	2.42 ± 0.082
4	5	1.1 ± 0.29	8.8 ± 0.68	7.90 ± 1.9	2.27 ± 0.157
20	5	0.95 ± 0.083	8.4 ± 0.44	8.77 ± 0.94	2.33 ± 0.141
50	5	1.2 ± 0.15	8.9 ± 0.79	7.62 ± 0.43	2.32 ± 0.173
80	5	1.1 ± 0.30	8.8 ± 0.91	8.30 ± 4.0	2.39 ± 0.121
4	8	0.85 ± 0.12	7.4 ± 0.18	8.67 ± 1.2	2.53 ± 0.120
20	8	0.98 ± 0.014	8.2 ± 0.30	8.42 ± 0.37	2.55 ± 0.112
50	8	0.93 ± 0.065	9.1 ± 0.58	9.81 ± 0.49	2.28 ± 0.193
80	8	1.1 ± 0.28	8.9 ± 0.38	8.27 ± 2.4	2.16 ± 0.068
4	10	0.93 ± 0.14	8.1 ± 0.31	8.71 ± 1.1	2.59 ± 0.028
20	10	1.1 ± 0.16	7.6 ± 0.094	7.19 ± 1.2	2.70 ± 0.114
50	10	1.3 ± 0.21	8.5 ± 0.83	6.80 ± 0.91	2.48 ± 0.055
80	10	1.2 ± 0.077	8.2 ± 0.71	7.02 ± 0.31	2.53 ± 0.045

Table 7 : Integral areas of Q_3, Q_4 and Q_4/Q_3 ratios calculated from the quantitative FTIR spectra and predicted Q_4/Q_3 ratios calculated by PLSR of *Thalassiosira weissflogi* diatom samples cleaned with H_2O_2 and aqua regia and treated with various temperature and time conditions.

***Thalassiosira weissflogii* diatom**		**Integral Area of Q_4/Q_3 in FTIR Spectra**			
		Q_3	Q_4	Q_4/Q_3	**Predicted Q_4/Q_3**
Temperature (˚C)	Time (days)	Peak centre: 945 cm^{-1} (Si – OH)	Peak centre: 800 cm^{-1} (O – Si – O)	(O – Si – O/ Si –OH)	(PLSR)
0	0	35	25	0.70	0.67
4	2	36 ± 0.87	27 ± 3.8	0.74 ± 0.71	0.90 ± 0.08
20	2	39 ± 1.9	28 ± 4.3	0.72 ± 0.45	0.82 ± 0.16
50	2	35 ± 4.9	26 ± 5.1	0.74 ± 1.3	0.84 ± 0.21
80	2	40 ± 3.6	32 ± 5.5	0.80 ± 0.53	0.90 ± 0.09
4	5	36 ± 1.4	30 ± 2.9	0.84 ± 1.9	1.05 ± 0.11
20	5	35 ± 3.0	26 ± 3.4	0.72 ± 0.94	0.93 ± 0.21
50	5	40 ± 0.38	25 ± 3.7	0.64 ± 0.43	0.96 ± 0.20
80	5	38 ± 3.8	27 ± 3.3	0.69 ± 4.0	1.22 ± 0.19
4	8	37 ± 0.60	27 ± 3.0	0.75 ± 1.2	0.97 ± 0.39
20	8	38 ± 0.95	28 ± 2.6	0.74 ± 0.37	0.85 ± 0.14
50	8	36 ± 2.1	30 ± 13	0.83 ± 0.49	1.04 ± 0.10
80	8	40 ± 2.7	32 ± 7.1	0.78 ± 2.4	1.07 ± 0.33
4	10	36 ± 1.6	23 ± 3.3	0.65 ± 1.1	0.64 ± 0.26
20	10	36 ± 3.6	29 ± 4.0	0.81 ± 1.2	0.76 ± 0.10
50	10	37 ± 2.7	35 ± 1.4	0.95 ± 0.91	1.20 ± 0.15
80	10	38 ± 1.7	27 ± 6.2	0.72 ± 0.31	0.80 ± 0.17

The Q_4/Q_3 ratios calculated by the integral areas for bamboo are significantly larger the than the predicted Q_4/Q_3 ratios calculated by PLSR (Table 6). By contrast, the Q_4/Q_3 ratios calculated by the integral areas for the diatom samples are slightly smaller the than the predicted Q_4/Q_3 ratios calculated by PLSR (Table 7).

The integral areas of Q_4 are ~5.5 times larger then the areas of Q_3 in bamboo samples whilst the integral areas of Q_4 are ~1.5 times smaller then the areas of Q_3 for the diatom samples.

The integral areas of Q_3 of bamboo are ~ 23 times smaller then the integral areas of Q_3 of diatom samples. The integral areas of Q_4 of bamboo is also ~ 3 times smaller then the integral areas of Q_4 of diatom samples.

The predicted Q_4/Q_3 ratios calculated by PLSR for bamboo samples are ~2.7 times larger then the areas predicted Q_4/Q_3 ratios of diatom samples.

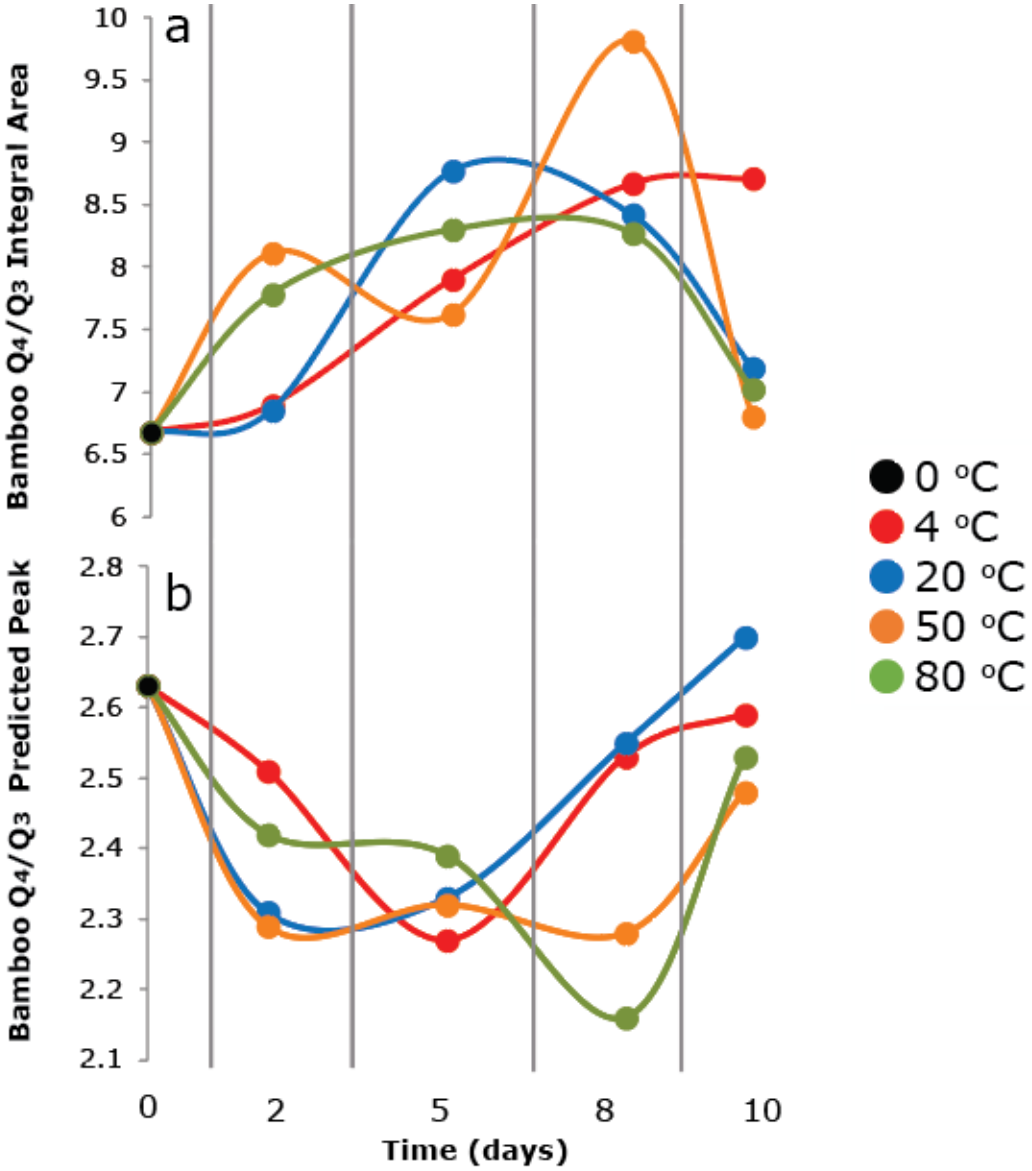

Figure 17: Comparison of (a) integral areas Q_4/Q_3 ratios calculated from the quantitative FTIR spectra and (b) predicted Q_4/Q_3 ratios calculated by PLSR of bamboo samples cleaned with H_2O_2 and aqua regia and treated with various temperature and time conditions. Multi-coloured dots represent (Black: t = 0, Red: 4˚C, Blue: 20˚C Orange: 50˚C, Green: 80˚C).

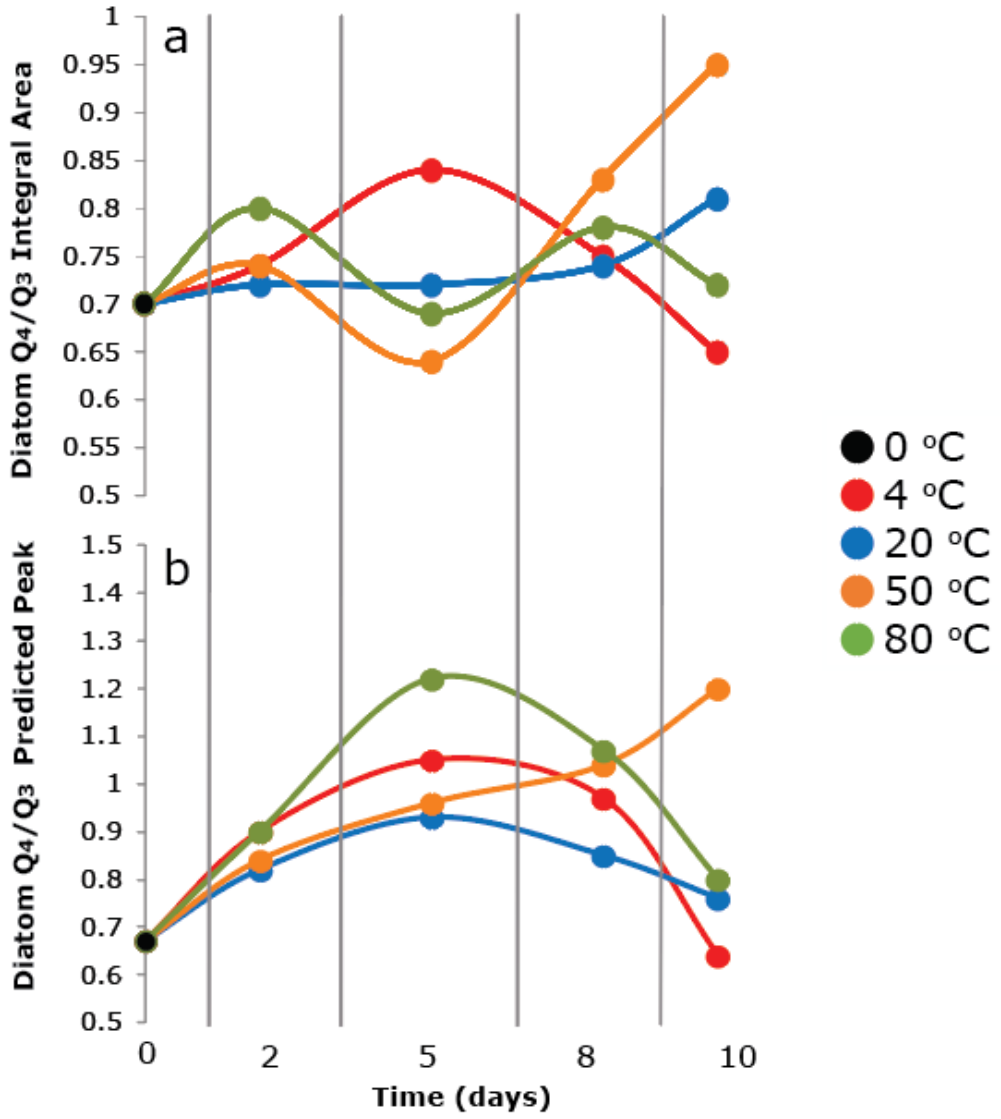

Figure 18 : Comparison of (a) integral areas Q_4/Q_3 ratios calculated from the quantitative FTIR spectra and (b) predicted Q_4/Q_3 ratios calculated by PLSR of *Thalassiosira weissflogi* diatom samples cleaned with H_2O_2 and aqua regia and treated with various temperature and time conditions. Multi-coloured dots represent (Black: t = 0, Red: 4˚C, Blue: 20˚C Orange: 50˚C, Green: 80˚C).

The trends of Q_4/Q_3 ratios calculated by the integral areas in bamboo increase with time, from 0, 2, 5 to 8 days. The trends then decrease after 10 days for all temperature variations, exept 4˚C, which doesn't change after 8 days (Fig. 17 a). There is a rapid increase over 0-2 days before trend at 80 ˚C plateaus and before trend at 50 ˚C decreases and then increases once more. By contrast, at lower temperatures, the trends do not start increasing until after 5 days, but the eventual change was nearly identical.

The trends of Q_4/Q_3 ratios calculated by PLSR for bamboo decrease with time from 0, 2 to 5 days. The trends then increase after 5 days for all temperature variations, but 80˚C, which increases after 8 days (Fig. 17 b). There are no other disenable changes in Q_4/Q_3 ratio trends for bamboo treated with different temperatures over time.

There are no discernible changes in Q_4/Q_3 ratio calculated by the integral areas in diatom samples treated with different temperatures over time (Fig. 18 a). The trends of Q_4/Q_3 ratios calculated by PLSR for diatom samples increase with time from 0, 2 to 5 days. The trends then decrease after 5 days for all temperature variations, but 50˚C, which continues to increase (Fig. 18 b).

4. DISCUSSION

This study set out to examine how the nature of BiSi within plant leaves and diatoms changed by common laboratory practices of heating over time. Various studies have suggested the condensation of silica is affected by temperature with time (Schmidt *et al.* 2001; Moschen *et al*. 2006; Dodd *et al.* 2012). This study calibrated FTIR to NMR reference samples to find a method of measuring silica condensation using FTIR. An experiment of changing temperature and time was implemented to investigate whether there is a positive correlation between BiSi condensation rate and temperature. FTIR spectra were obtained and analysed by various statistical analyses techniques. However, structural analysis is complicated by organic material in BiSi. Various treatments were tested and applied to remove organics as a means to attain pure silica samples, however residual organic contamination appears to have had a confounding effect on these experiments.

4.1. Performance of calibrated FTIR and NMR model

The small difference in the R^2 coefficient of determination between calibrated and external validation sample sets indicates a confident estimation in the calibration (Fig. 4). The model developed in this study to predict the degree of hydration Q_4/Q_3 can be used with confidence, with the assumption that organic material is not contaminating FTIR spectra.

FTIR spectroscopy is a conveniently fast and cheap analycal techique which measures the Q_4 and Q_3 signal intensities, in comparison to NMR. However, FTIR spectra are not as quantitative as the spectra obtained through NMR. Other studies have also suggested potential in the application of FTIR analysis (Bertermann *et al.*, 2003; Gendron-Badou *et al.*, 2003). A particular limitation of FTIR is its sensitivity to organic contamination, which can obscure the observation and quantification of infra red peaks of interest, whether or not the contamination are near silica peaks or elsewhere in the spectrum (Fig. 9, 10).

Previous studies that measure Q_4/Q_3 ratios use ^{29}Si NMR data whereas this study made Q_4/Q_3 ratio measurements from FTIR (Bertermann *et al.*, 2003; Gendron-Badou *et al.*, 2003; Leng *et al.*, 2009). The relative peak intensities of FTIR and NMR are not relatable because these measures are relative to the specific variables of the machineary measuring molecular resonances. So a comparison between literature measured Q_4/Q_3 ratios and the Q_4/Q_3 ratios measured in this study is not possible.

4.2. Selection of Treatment Method

This study investigated a variety of treatments used to find an optimal method in removing organic material (Table 2). Many studies follow standard treatments used to

remove organic material in diatoms (Morley *et al.*, 2004, Xiong & Crosta, 2012). Tyler *et al.* (2007) suggested that diatoms treated in H_2O_2 for 30 hours is equivalent to removing organics via ignition in air at 550˚C. Digestion in H_2O_2 does not affect $\delta^{18}O_{silica,}$ although Tyler *et al.* (2007) used Miocene aged diatomite which may have undergone silica condensation and would not be as hydrated as the fresh diatoms used in this study. The analysis of the silica structure may be further complicated due to the prolonged use of H_2O_2 which may cause solidificaion of BiSi and would negate the effects of other additional oxidative techniques used to remove organics (Tyler *et al.*, 2007). In this study, H_2O_2 removed sufficient organic material (~1.5% residual carbon) in diatom samples. It is also the most favourable treatment to use as it is the least invasive technique. However, this is not the case for the phytolith samples which contain a significantly higher amount of residual organic material ~40% compared to diatoms (Fig. 5-8).

Another standard reagent used to remove organic material in diatoms is aqua regia ($HNO_3/HClO_4$) (Shemesh *et al.*, 1995; Shemesh *et al.*, 2001; Rosqvist *et al.*, 2004). However, Watling *et al.* (2011) suggested that 30% of remaining total nitrogen within phytolith samples can be attributed to the addition of nitrogen during acid hydrolysis by using HNO_3 as a pre-treatment method. This would be unfavourable because additional nitrogen can contaminate the FTIR spectra and create overlap of signals used to measure silica. Treatments with aqua regia showed smoothing of contaminating organic peaks in the FTIR spectra which makes this treatment favourable (Fig. 9, 10). Although, this treatment causes borderline "over-smoothing" in the FTIR spectra of diatoms (Fig. 10).

$BaCl_2$ is a common solution used to remove organic material in soils by cation-exchange reactions (Lax, Roig & Costa, 1986). The cation-exchange occurs during oxidation and hydrolysis where Ba^+ exchanges with NH_3^+, binding to SiO^-, which reduces the quantity of contaminating nitrogen in the sample (Fig. 19). Barium contaminates the sample instead of nitrogen but it is not an issue since the ion does not influence FTIR spectra. However, in this study, there was no effect of $BaCl_2$ solution in removing organic material (Fig. 9, 10). This outcome may be due to solidification of BiSi that occurred during H_2O_2 oxidation (Tyler *et al*., 2007), prior to the pre-treatment of $BaCl_2$, which hindered cation-exchange within the silica matrix.

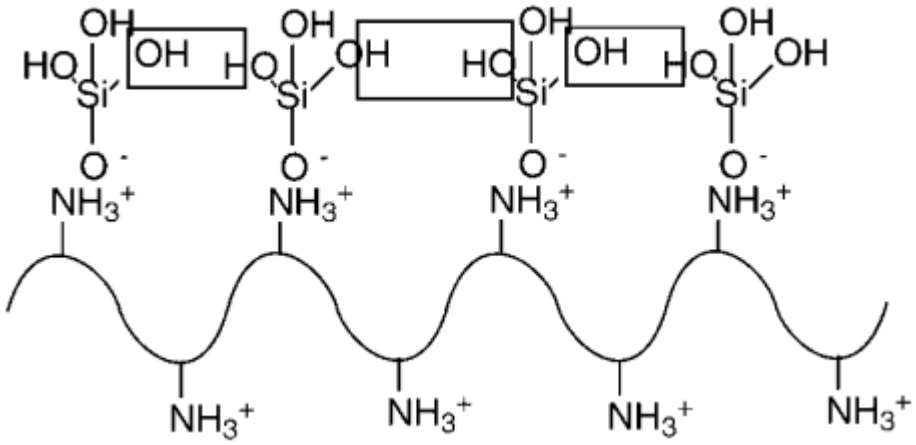

Figure 19: Modified figure from Coradin & Lopez, (2003) showing the interaction of silicates with ammonium groups found in molecules, such as, proteins.

Photo-oxidation is a technique used to create highly oxidative radicals (OH*) with the source of UV radiation. These radicals have the potential to mineralise organic material, with the potential limitation that it can not oxidise material deeper than the surface (Sanly et al., 2007). Photo-oxidation was an effect technique at eliminating organic material. However, it managed to degrade the most of the entirety of the sample which is extremely unfavourable (Fig. 9). Photo-oxidisation is also fundamentally limited by

the size of the sample that can be prepared, so whilst it is relatively quick and effective, it wasn't chosen as a viable technique for further application in this study.

Respectively, the differences in organic content between additional oxidative treatments applied after H_2O_2 digestion, with the exception of photo-oxidation, is small enough to be negligible. However, aqua regia does not react violently and explosively with sediments or organic rich materials, as can be the case with H_2O_2. Despite several reservations surrounding each of the techniques examined, the combination of H_2O_2 and aqua regia (Treatment 2) was chosen as the best technique for organic removal in subsequent experiments. Treatment 2 was conducted on all samples to maintain consistent methodology throughout the experiments.

4.3. Effectiveness of the Purification of phytolith and diatom samples

The bamboo samples analysed in this study, even after pre-treatment, were found to be excessively high in organic contaminants compared to the diatoms. The most abundant contaminant present in phytolith samples was cellulose (Fig. 7, 8). In the solid state, cellulose has a strong attraction to water and the disordered structure of these macromolecules can be easily hydrated (Kačuráková *et al.*, 2000). This raises issues because, not only does additional material to silica confuse the structural analysis of silica, but the cellulose in phytolith samples can absorb and release water which may alter the overall hydration of silica.

The high concentration of cellulose contamination suggests that the pre-treatment may have had little to no effect at removing any cellulose from phytolith sample (Fig. 7, 8). Progressive oxidation may be more effective at breaking down weaker structures such as silica but results in mass accumulation of resilient residuals with stronger bonded

waxy organics and cellulose. This may explain why we observe exceptionally smaller values for the integral areas of Q_3 and Q_4 in bamboo, compared to diatom samples (Table 7, 8). Nevertheless, treated bamboo phytoliths consist of ~85% pure phytolith silica, whereas, treated diatom samples contain purely ~100% silica (Chapligin *et al*. 2011; Kamenik, Mizera & Randa, 2013; Anala & NamBiSian, 2015). Thus, it is expected that diatoms would have larger Si–O–Si/ Si–OH peaks in FTIR. However, the studies outlining the consentrations of pure silica were obtained by acid digestion and incineration (Chapligin *et al*., 2011; Kamenik, Mizera & Randa, 2013; Anala & NamBiSian, 2015).

Kamenik, Mizera & Randa (2013) conducted a study on phytolith extracting methods and found that the sole use of acid digestion, similarly used in this study, is inefficient in removing all organic material. The study suggested acid treatment followed by incineration is most effective (Kamenik, Mizera & Randa, 2013). However, this is an unfavourable method since incinerating samples would defeat the purpose of this study to observe the effects of heating on the changes in BiSi structure. Hodson (2016) suggests that cellulose acts as a template for silica deposition in the cell walls, cell plates and stomata. This study supports those observations by indicating that organic material is locked into the silicified structure of phytoliths which would complicate alternative pre-treatment methods (Hodson, 2016).

The remaining organic contamination in diatom samples is small (Fig. 5, 6). The relative ease of removing organic contaminants from diatoms is most likely due the high surface area produced by the intricate silica pattern (Fig. 3, 20).

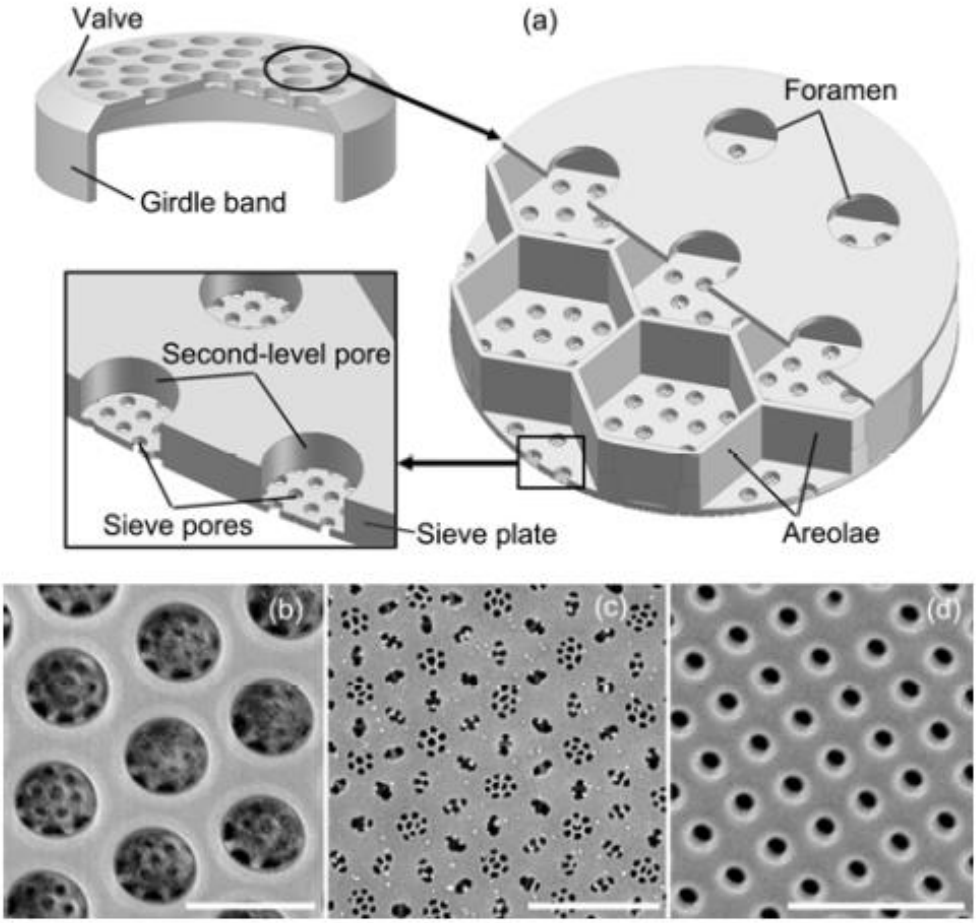

Figure 20: Modified figure from Zhang *et al.* (2012) showing the muti-level pore system of *Coscinodisus sp.* (a) 3D model similar to structure of SEM images in Fig. 3 (b) forarm and second level pores, scale bar 1 µm; (c) sieve pore, scale 2 µm; (d) girdle band non-nano porous sturcture, scale 1 µm.

4.4. Comparison of structural change in BiSi Q_4/Q_3 ratios by heating and time

Two methods were used to measure BiSi Q_4/Q_3 ratios bamboo and *Thalassiosira weissflogi* diatoms samples (Table 6, 7): by calculating the integral areas of Q_4 and Q_3 in FTIR spectra and by predicting Q_4/Q_3 ratios calculated by PLSR (Fig. 17, 18). There are no discernible correlations between integrated Q_4/Q_3 peak areas and the Q_4/Q_3 ratios calculated from the calibrated FTIR spectra, for neither bamboo or diatom samples. This study suggests that the optimal method for measuring Q_4/Q_3 ratios may be dependant on

the variability of remaining impurities in sample or the additional contaminants present in FTIR spectral peaks.

The remaining impurities in bamboo that impact the purification of BiSi also affects the statistical analysis that follows experimentation. Organic matter within BiSi samples is widespread and not isolated to specific parts of FTIR spectra. Thus, spectral peaks representing Q_4 and Q_3 would have a mixture of organic and silica contents (Fig. 11, 12). Conflicting evidence, already discussed, indicates that there is the presence of organics that contaminate the calibration of FTIR, which would affect the calculations used to model PLSR Q_4/Q_3 predictions (Table 6, 7). The key uncertainties with PLSR is that peaks with a spectrum must be relatively similar, which is not the case with bamboo samples that contain many other peaks related to cellulose in the spectra (Fig. 9a). This leads to the interpretation that the peak integration technique is a more robust method for bamboo (Fig. 17 a).

The peak integration technique is not as useful at measuring Q_4/Q_3 ratios for diatom samples as it is for the bamboo samples. Despite the insignificant organic content remaining after pre-treatment of diatoms, the specific FTIR spectra peaks related to Si–OH and Si–O–Si are filled abundantly with additional contaminant peaks (Fig. 13, 14). This indicates that additional contaminants would have a dominating effect on calculating Q_4/Q_3 integral peak areas (Table 5, 6). Thus, the PLSR calibrated FTIR technique is a better method to measuring Q_4/Q_3 ratios for diatom samples (Fig. 18 b).

Furthermore, PCA analysis incorporates all wavelengths in FTIR spectra and the presence of organic residuals and additional contaminant peaks may be a reason why no correlation was found in PCA analysis (Fig. 15, 16).

According to this study, Q_4/Q_3 can be measured by using integral Q_4/Q_3 FTIR peak areas for bamboo (Fig. 17 a) and Q_4/Q_3 PLSR calibrated FTIR for diatoms (Fig. 18 b). These two techniques used to measure Q_4/Q_3 ratios in bamboo and diatoms show similar patterns in the trends observed in Fig. 17a and Fig. 18b. Both Q_4/Q_3 plots exhibit an increase and then decrease in Q_4/Q_3 ratios over the course of the 10 day experiment. The increase in Q_4/Q_3 represents dehydroxylation (the removal of silanol groups from the silica surface), and the decrease represents rehydroxylation (restoration of hydroxyls) in the silica structure.

These results do agree with the main hypothesis of the study, where there is a positive relationship of silica condensation through time, but there is no distinct and lasting effect of heating for a period over 10 days. The Q_4/Q_3 pattern of condensation is reversed, implying that there is a rehydration after 8 days for bamboo and after 5 days for diatoms (Fig. 17 a, 18 b). One interpretation for the time difference in rehydration is that diatoms have a larger surface area which allows more surface reactions to occur than on the uniform bamboo surface (Fig. 3, 20). Another interpretation is that bamboo contains tough organic material which takes longer to digest than silica and requires a greater activation barrier to undergo rehydration. This leads to the question as to whether the reversal of hydration reaction is due to either further loss of organic coating or breaking of mineral surface to enhance absorption. By contrast, other studies, such as Dodd *et al.,* (2012), suggested that the Si–OH content decreases as a result of maturation during condensation (Eq. 1). The maturation process is assumed to be constant and diatoms could reach near equilibrium silica-water compositions within half a year after diatom death (Dodd *et al.,* 2012). However, this study suggests that the Q_4/Q_3 structure of silica doesn't remain constant in water and alterations in the structure

of silica through condensation reaction is reversible after just 10 days. The results of this study also do not show a relationship between the rate and the total amount of change with temperature. After 10 days the Q_4/Q_3 values revert back to their initial Q_4/Q_3 values from t=0 (Fig. 17 a, 18 b).

4.5. Improvements and further research

The various oxidative technique used to remove organic material from silica should be revised and explored further. For example, the probability of silica solidification caused by treatment with H_2O_2 needs to me minimised throughout the pre-treatment of silica. The method should instead involve various oxidative techniques simultaneously used with hot H_2O_2 as a means to optimise organic removal during the oxidation process before silica has the time to harden. This method may be particularly more effective using the $BaCl_2$ pre-treatment which, in this study, BiSi may not have been able to undergo cation-exchange due to sturctural solidification.

Further research is particularly needed to remove a greater quantity of organic material in phytolth samples. Perhaps a longer duration of sample digestion in hot aqua regia may reduce the organic material in phytoliths. However, the problem with altering this method raises concerns that silica matrix will also be dissolved during digestion of organic material. Alele & Ulbricht, (2016) used a membrane-based purification method to create nano-particle dispersions of proteins in organic/inorganic hybrid systems using ultrafiltration. In future research, an adaption of this method may be able to separate cellulose from silica during oxidation.

The diatom samples remained congealed together and were not in a usual dry-powdered form, even after prolonged drying of samples in a freeze dryer. This may indicate that

freeze drying is not sufficient to dry diatom samples and it may be the reason why diatoms contain many additional contamination peaks in FTIR (Fig. 13, 14). Further investigation is required to understand the reason behind this unusual sample texture. If the method freeze drying is the origin of the issue, an alternative method is required to remove water from sample. Perhaps using liquid-nitrogen as an alternative method to dry samples is a possible area for further research to explore. If the method freeze drying is the not the origin of the issue, then maybe the methodology of putting samples in water is an alternative area of future research. This is based on the results which show that silica undergoes re-absorption of -OH in silica (Fig. 17, 18). A method which involves no water-silica interactions maybe conducted by placing silica samples in tubes at different temperature without the presence of water.

Addition experiments are needed to test whether the method of measuring the integral peaks in FTIR of Q_4/Q_3 is in fact a reliable technique. However, these experiments will need to be compared with FTIR peak standards to ensure accuracy of measurements.

5. CONCLUSIONS

On the basis of the experiments conducted in this study there appears to be a relationship between time and the relative dehydroxylation of biogenic silica. This was observed using different methods for measuring the structure of silica, where integral peaks in FTIR was a more comprehensive model for bamboo and a PLSR calibrated FTIR model was a more comprehensive model for diatoms. Contrary to the original hypothesis, the condensation reaction causing the relative reduction of hydration of biogenic silica with time is reversible after 10 days and reverts back to their original Q_4/Q_3 values when t=0. These results imply that the silica does not undergo progressive condensation but a possible temporary absorption/desorption on the surface of silica.

However, several methodological issues related to residual impurities which potentially undermine these results effecting how Q_4/Q_3 is measured. There is therefore a need to acquire a better understanding of both approaches to organic removal in biogenic silica, in addition to methods which allow quantifiable measurements of changes in the structure of silica.

ACKNOWLEDGMENTS

I would like to thank first and foremost, my supervisor, Dr Jonathan Tyler, for his guidance and enthusiasm for my work this year. I would also like to thank Dr. Bruce Hawke and Dr. Jeff Baldock at CSRIO, Soil and Water, for their assistance in laboratory work to obtain NMR and FTIR spectra, informative discussions and assistance with statistical analysis throughout the year. I would also like to thank Dr. Ursula Langride-Remold from the School of Agriculture, Food and Wine, University of Adelaide, for the supplying wheat samples for this project. The staff at Fern Forest Nursery -Willunga for donating bamboo samples. I would like to thank Lyn Waterhouse at Adelaide Microscopy for her assistance with SEM imaging and enthusiasm.

REFERENCES

ALELE, N., & ULBRICHT, M. (2016). Membrane-based purification of proteins from nanoparticle dispersions: Influences of membrane type and ultrafiltration conditions. *Separation and Purification Technology, 158*, 171-182. doi: http://dx.doi.org/10.1016/j.seppur.2015.11.031

ANALA, R., & NAMBISIAN, P. (2015). Study of morphology and chemical composition of phytoliths on the surface of paddy straw. *Paddy and Water Environment, 13*(4), 521-527. doi: 10.1007/s10333-014-0468-5

BERTERMANN, R., KRÖGER, N., & TACKE, R. (2003). Solid-state 29Si MAS NMR studies of diatoms: structural characterization of biosilica deposits. *Analytical and Bioanalytical Chemistry, 375*(5), 630-634. doi: 10.1007/s00216-003-1769-5

BRANDRISS, M. E., O'NEIL, J. R., EDLUND, M. B., & STOERMER, E. F. (1998). Oxygen Isotope Fractionation Between Diatomaceous Silica and Water. *Geochimica et Cosmochimica Acta, 62*(7), 1119-1125. doi: http://dx.doi.org/10.1016/S0016-7037(98)00054-4

CHAPLIGIN, B., LENG, M. J., WEBB, E., ALEXANDRE, A., DODD, J. P., IJIRI, A., YAM, R. (2011). Inter-laboratory comparison of oxygen isotope compositions from biogenic silica. *Geochimica et Cosmochimica Acta, 75*(22), 7242-7256. doi: http://dx.doi.org/10.1016/j.gca.2011.08.011

CORADIN, T., & LOPEZ, P. J. (2003). Biogenic Silica Patterning: Simple Chemistry or Subtle Biology? *ChemBioChem, 4*(4), 251-259. doi: 10.1002/cbic.200390044

DEGENS, E. T., & EPSTEIN, S. (1962). Relationship between O 18 /O 16 ratios in coexisting carbonates, cherts, and diatomites. *AAPG Bulletin, 46*(4), 534-542.

DING, T. P., ZHOU, J. X., WAN, D. F., CHEN, Z. Y., WANG, C. Y., & ZHANG, F. (2008). Silicon isotope fractionation in bamboo and its significance to the biogeochemical cycle of silicon. *Geochimica et Cosmochimica Acta, 72*(5), 1381-1395. doi: http://dx.doi.org/10.1016/j.gca.2008.01.008

DODD, J. P., SHARP, Z. D., FAWCETT, P. J., BREARLEY, A. J., & MCCUBBIN, F. M. (2012). Rapid post-mortem maturation of diatom silica oxygen isotope values. *Geochemistry, Geophysics, Geosystems, 13*(9), n/a-n/a. doi: 10.1029/2011GC004019

DOLININA, E. S., & PARFENYUK, E. V., (2014). The effects of surface chemistry of mesoporous silica materials and solution pH on kinetics of molsidomine adsorption. *Journal Name: Journal of Solid State Chemistry; Journal Volume: 209; Other Information: Copyright (c) 2013 Elsevier Science B.V., Amsterdam, The Netherlands, All rights reserved.; Country of input: International Atomic Energy Agency (IAEA)*, Medium: X; Size: page(s) 105-112.

Filippov. M.P (1992). Practical infrared spectroscopy of pectic substances. *Food Hydrocolloids, 6*(1), 115-142. doi: http://dx.doi.org/10.1016/S0268-005X(09)80060-X

FREDLUND, G. G. (1993). Paleoenvironmental interpretations of stable carbon, hydrogen, and oxygen isotopes from opal phytoliths, Eustis Ash Pit, Nebraska. *MASCA research papers in science and archaeology, 10*, 37-46.

GENDRON-BADOU, A. C., CORADIN, T., MAQUET, J., FRÖHLICH, F., & LIVAGE, J. (2003). Spectroscopic characterization of biogenic silica. *Journal of Non-Crystalline Solids, 316*(2–3), 331-337. doi: http://dx.doi.org/10.1016/S0022-3093(02)01634-4

GRAETSCH, H. (1994). Structural characteristics of opaline and microcrystalline silica minerals. *Reviews in Mineralogy and Geochemistry, 29*(1), 209-232.

GRÖGER, C., SUMPER, M., & BRUNNER, E. (2008). Silicon uptake and metabolism of the marine diatom Thalassiosira pseudonana: Solid-state 29Si NMR and fluorescence microscopic studies. *Journal of Structural Biology, 161*(1), 55-63. doi: http://dx.doi.org/10.1016/j.jsb.2007.0

HODSON, M. J. (2016). The development of phytoliths in plants and its influence on their chemistry and isotopic composition. Implications for palaeoecology and archaeology. *Journal of Archaeological Science, 68*, 62-69. doi: http://dx.doi.org/10.1016/j.jas.2015.09.002

HODSON, M. J., PARKER, A. G., LENG, M. J., & SLOANE, H. J. (2008). Silicon, oxygen and carbon isotope composition of wheat (Triticum aestivum L.) phytoliths: implications for palaeoecology and archaeology. *Journal of Quaternary Science, 23*(4), 331-339. doi: 10.1002/jqs.1176

KAČURÁKOVÁ, M., CAPEK, P., SASINKOVÁ, V., WELLNER, N., & EBRINGEROVÁ, A. (2000). FT-IR study of plant cell wall model compounds: pectic polysaccharides and hemicelluloses. *Carbohydrate Polymers, 43*(2), 195-203. doi: http://dx.doi.org/10.1016/S0144-8617(00)00151-X

KAMMER, M., HEDRICH, R., EHRLICH, H., POPP, J., BRUNNER, E., & KRAFFT, C. (2010). Spatially resolved determination of the structure and composition of diatom cell walls by Raman and FTIR imaging. *Analytical & Bioanalytical Chemistry, 398*(1), 509-517. doi: 10.1007/s00216-010-3924-0

KNAUTH, L. P., & EPSTEIN, S. (1982). The nature of water in hydrous silica. *American Mineralogist, 67*(5-6), 510-520.

LABEYRIE, L. D. (1974), New approach to surface seawater paleotemperatures using 18O/16O ratios in silica of diatom frustules, Nature, 248, 40-42.

LABEYRIE, L. (1972), Composition isotopique de l'oxygène de la silice biogenique., C.R. Acad. Sc. Paris, 1605-1608.

LABEYRIE, L. D., & JUILLET, A. (1982). Oxygen isotopic exchangeability of diatom valve silica; interpretation and consequences for paleoclimatic studies. *Geochimica et Cosmochimica Acta, 46*(6), 967-975. doi: http://dx.doi.org/10.1016/0016-7037(82)90052-7

LAX, A., ROIG, A., & COSTA, F. (1986). A method for determining the cation-exchange capacity of organic materials. *Plant and Soil, 94*(3), 349-355. doi: 10.1007/BF02374329

LECOMTE, J. (1949). Le Rayonnement Infrarouge. Paris: Gauthier-Villars, p. 752

LENG, M. J., & HENDERSON, A. C. G. (2013). Recent advances in isotopes as palaeolimnological proxies. *Journal of Paleolimnology, 49*(3), 481-496. doi: 10.1007/s10933-012-9667-5

LENG, M. J., SWANN, G. E. A., HODSON, M. J., TYLER, J. J., PATWARDHAN, S. V., & SLOANE, H. J. (2009). The Potential use of Silicon Isotope Composition of Biogenic Silica as a Proxy for Environmental Change. *Silicon, 1*(2), 65-77. doi: 10.1007/s12633-009-9014-2

LENG, M. J., & SLOANE, H. J. (2008). Combined oxygen and silicon isotope analysis of biogenic silica. *Journal of Quaternary Science, 23*(4), 313-319. doi: 10.1002/jqs.1177

LENG, M. J., & BARKER, P. A. (2006). A review of the oxygen isotope composition of lacustrine diatom silica for palaeoclimate reconstruction. *Earth Science Reviews, 75*(1), 5-27. doi: 10.1016/j.earscirev.2005.10

MATHENEY, R. K., & KNAUTH, L. P. (1989). Oxygen-isotope fractionation between marine biogenic silica and seawater. *Geochimica et Cosmochimica Acta, 53*(12), 3207-3214. doi: http://dx.doi.org/10.1016/0016-7037(89)90101-4

MEYER-JACOB, C., VOGEL, H., BOXBERG, F., ROSÉN, P., WEBER, M. E., & BINDLER, R. (2014). Independent measurement of biogenic silica in sediments by FTIR spectroscopy and PLS regression. *Journal of Paleolimnology, 52*(3), 245-255. doi: 10.1007/s10933-014-9791-5

MOENKE, H.H.W.(1974). *The Infrared Spectra of Minerals*. London: Mineralogical Society of Great Britain and Ireland, (4), 365. doi:10.1180/mono-4.

MOPPER, K., & GARLICK, G. D. (1971). Oxygen isotope fractionation between biogenic silica and ocean water. *Geochimica et Cosmochimica Acta, 35*(11), 1185-1187. doi: http://dx.doi.org/10.1016/0016-7037(71)90032-9

MORLEY, D. W., LENG, M. J., MACKAY, A. W., SLOANE, H. J., RIOUAL, P., & BATTARBEE, R. W. (2004). Cleaning of lake sediment samples for diatom oxygen isotope analysis. *Journal of Paleolimnology, 31*(3), 391-401. doi: 10.1023/B:JOPL.0000021854.70714.6b

MOSCHEN, R., LÜCKE, A., PARPLIES, J., RADTKE, U., SCHLESER, G.H. (2006). Transfer and early diagenesis of biogenic silica oxygen isotope signals during settling and sedimentation of diatoms in a temperate freshwater lake (Lake Holzmaar, Germany). *Geochimica et Cosmochimica Acta, 70*(17), 4367-4379. doi: 10.1016/j.gca.2006.07.001

MOSCHEN, R., LÜCKE, A., SCHLESER, G.H. (2005). Sensitivity of biogenic silica oxygen isotopes to changes in surface water temperature and palaeoclimatology. *Geophysical Research Letters, 32*(7), L07708. doi: 10.1029/2004GL022167

NEETHIRAJAN, S., GORDON, R., & WANG, L. (2009). Potential of silica bodies (phytoliths) for nanotechnology. *Trends in Biotechnology, 27*(8), 461-467. doi: http://dx.doi.org/10.1016/j.tibtech.2009.05.002

PARKE, S. (1974). *The Infrared Spectra of Minerals*. London: Mineralogical Society of Great Britain and Ireland, (4), 483. doi:10.1180/mono-4.

PERRY, C. C. (2003). Silicification: The Processes by Which Organisms Capture and Mineralize Silica. *Reviews in Mineralogy and Geochemistry, 54*(1), 291-327. doi: 10.2113/0540291

ROSQVIST, G., JONSSON, C., YAM, R., KARLÉN, W., & SHEMESH, A. (2004). Diatom oxygen isotopes in pro-glacial lake sediments from northern Sweden: a 5000 year record of atmospheric circulation. *Quaternary Science Reviews, 23*(7–8), 851-859. doi: http://dx.doi.org/10.1016/j.quascirev.2003.06.009

SANDERMAN, J., BALDOCK, J., HAWKE, B., MACDONALD, L., MASSIS-PUUCCINI, A., SZARVAS, STEVE,. (2011). National Soil and Carbon Research Programme : Field and laboratory Methodologies. National Research Flagships Sustainable Agriculture, CSIRO

SANLY, LIM, M., CHIANG, K., AMAL, R., FABRIS, R., CHOW, C., & DRIKAS, M. (2007). A Study on the Removal of Humic Acid Using Advanced Oxidation Processes. *Separation Science and Technology, 42*(7), 1391-1404. doi: 10.1080/01496390701289799

SCHMIDT, M., BOTZ, R., RICKERT, D., BOHRMANN, G., HALL, S. R., & MANN, S. (2001). Oxygen isotopes of marine diatoms and relations to opal-A maturation1. *Geochimica et Cosmochimica Acta, 65*(2), 201-211. doi: http://dx.doi.org/10.1016/S0016-7037(00)00534-2

SCHMIDT, M., BOTZ, R., STOFFERS, P., ANDERS, T., & BOHRMANN, G. (1997). Oxygen isotopes in marine diatoms: A comparative study of analytical techniques and new results on the isotope composition of recent marine diatoms. *Geochimica et Cosmochimica Acta, 61*(11), 2275-2280. doi: http://dx.doi.org/10.1016/S0016-7037(97)00081-1

SHEMESH, A., RIETTI-SHATI, M., RIOUAL, P., BATTARBEE, R., DE BEAULIEU, J.-L., REILLE, M., . . . SVOBODOVA, H. (2001). An oxygen isotope record of lacustrine opal from a European Maar indicates climatic stability during the Last Interglacial. *Geophysical Research Letters, 28*(12), 2305-2308. doi: 10.1029/2000GL012720

SHEMESH, A., BURCKLE, L. H., & HAYS, J. D. (1995). Late Pleistocene oxygen isotope records of biogenic silica from the Atlantic sector of the Southern Ocean. *Paleoceanography, 10*(2), 179-196. doi: 10.1029/94PA03060

Skjemstad, J. O, Taylor, J. A. and Blows, G. (1994). The construction and operation of a high energy UV photo-oxidiser for the investigation of carbon distribution in soil microaggregates. CSIRO Divisional report N124.

SWANN, G. E. A., & LENG, M. J. (2009). A review of diatom δ18O in palaeoceanography. *Quaternary Science Reviews, 28*(5–6), 384-398. doi: http://dx.doi.org/10.1016/j.quascirev.2008.11.002

TYLER, J. J., LENG, M. J., SLOANE, H. J., SACHSE, D., & GLEIXNER, G. (2008). Oxygen isotope ratios of sedimentary biogenic silica reflect the European transcontinental climate gradient. *Journal of Quaternary Science, 23*(4), 341-350. doi: 10.1002/jqs.1172

TYLER, J. J., LENG, M. J., & SLOANE, H. J. (2007). The effects of organic removal treatment on the integrity of δ18O measurements from biogenic silica. *Journal of Paleolimnology, 37*(4), 491-497. doi: 10.1007/s10933-006-9030-9

WATLING, K. M., PARR, J. F., RINTOUL, L., BROWN, C. L., & SULLIVAN, L. A. (2011). Raman, infrared and XPS study of bamboo phytoliths after chemical digestion. *Spectrochimica Acta Part A: Molecular and Biomolecular Spectroscopy, 80*(1), 106-111. doi: http://dx.doi.org/10.1016/j.saa.2011.03.002

WEBB, E. A., & LONGSTAFFE, F. J. (2000). The oxygen isotopic compositions of silica phytoliths and plant water in grasses: implications for the study of paleoclimate. *Geochimica et Cosmochimica Acta, 64*(5), 767-780. doi: http://dx.doi.org/10.1016/S0016-7037(99)00374-9

WOLD, S., SJÖSTRÖM, M., & ERIKSSON, L. (2001). PLS-regression: a basic tool of chemometrics. *Chemometrics and Intelligent Laboratory Systems, 58*(2), 109-130. doi: http://dx.doi.org/10.1016/S0169-7439(01)00155-1

XIONG, Z., LI, T., & CROSTA, X. (2012). Cleaning of marine sediment samples for large diatom stable isotope analysis. *Journal of Earth Science, 23*(2), 161-172. doi: 10.1007/s12583-012-0241-x

ZHANG, D., WANG, Y., CAI, J., PAN, J., JIANG, X., & JIANG, Y. (2012). Bio-manufacturing technology based on diatom micro- and nanostructure. *Chinese Science Bulletin, 57*(30), 3836-3849. doi: 10.1007/s11434-012-5410-x

ZHURAVLEV, L. T. (2000). The surface chemistry of amorphous silica. Zhuravlev model. *Colloids and Surfaces A: Physicochemical and Engineering Aspects, 173*(1–3), 1-38. doi: http://dx.doi.org/10.1016/S0927-7757(00)00556-2

APPENDIX A: RAW SPECTRAL DATA AND SPECTRAL ANALYSIS

All FTIR spectra is in electronic copy held with the supervisors of this project.

Table 1: Raw data of carbon content in samples treated in different organic digestion methods.

Treatment Type	C (mg/g)	N (mg/g)	C/N
Wheat H_2O_2	454.21	4.9	92.75
Bamboo H_2O_2	389.49	3.7	105.15
Thalassiosira pseudonana H_2O_2	14.99	0.22	69.39
1800 H_2O_2	9.08	NA	NA
Wheat H_2O_2 +aqua regia (1:3 HNO_3/HCl) + $BaCl_2$ salt solution	434.27	4.58	94.72
Bamboo H_2O_2 +aqua regia (1:3 HNO_3/HCl) + $BaCl_2$ salt solution	330.81	3.80	87.15
Thalassiosira pseudonana, H_2O_2 +aqua regia (1:3 HNO_3/HCl) + $BaCl_2$ salt solution	12.76	0.17	76.64
Thalassiosira weissflogii H_2O_2 +aqua regia (1:3 HNO_3/HCl) + $BaCl_2$ salt solution	11.58	0.06	196.74
Wheat aqua regia (1:3 HNO_3/HCl)	441.64	4.47	98.90
Bamboo aqua regia (1:3 HNO_3/HCl)	374.43	3.97	94.42
Thalassiosira pseudonana aqua regia (1:3 HNO_3/HCl)	15.99	0.21	77.79
Thalassiosira weissflogii aqua regia (1:3 HNO_3/HCl)	11.81	NA	NA
Wheat H_2O_2 + $BaCl_2$ salt solution	445.52	4.58	97.20
Bamboo H_2O_2 + $BaCl_2$ salt solution	383.95	3.67	104.52
Thalassiosira pseudonana H_2O_2 + $BaCl_2$ salt solution	14.73	0.30	48.75
Thalassiosira weissflogii H_2O_2 + $BaCl_2$ salt solution	10.22	NA	NA

Table 2: Total intensity NMR signals (%) of functional groups present in samples treated in different organic digestion methods

Treatment Type	0 - 45 Alkyl	45 - 60 N-Alkyl/Methoxyl	60 - 95 O-Alkyl	95 - 110 Di-O-Alkyl	110 - 145 Aryl	145 - 165 O-Aryl	165 - 215 Amide/Carboxyl
Bamboo	21.5	3.4	50.3	10.3	5.2	2.3	7.1
Wheat	8.5	2	65.5	14.2	3.9	1.7	4.2
Bamboo 2 hour photo-oxidation	13.8	2.3	61.9	13	3.8	1.5	3.6
Bamboo 4 hour photo-oxidation	11.1	1.9	64.7	13.5	3.5	1.4	3.8
Wheat 2 hour photo-oxidation	8.1	1.9	67.8	14.2	3.6	1.3	3.1
Wheat 4 hour photo-oxidation	8	1.7	66.1	14.1	4.1	1.9	4.1

Figure 1: A comparison Principle component analysis (PCA) plots bamboo samples cleaned with H_2O_2 and aqua regia at various times of (a) 4 ˚C (b) 20 ˚C (c) 50 ˚C (d) 80 ˚C. Multi-coloured dots represent (Black: t = 0, Red: 2 days, Blue: 5 days, Orange: 8 days, Green: 10 days).

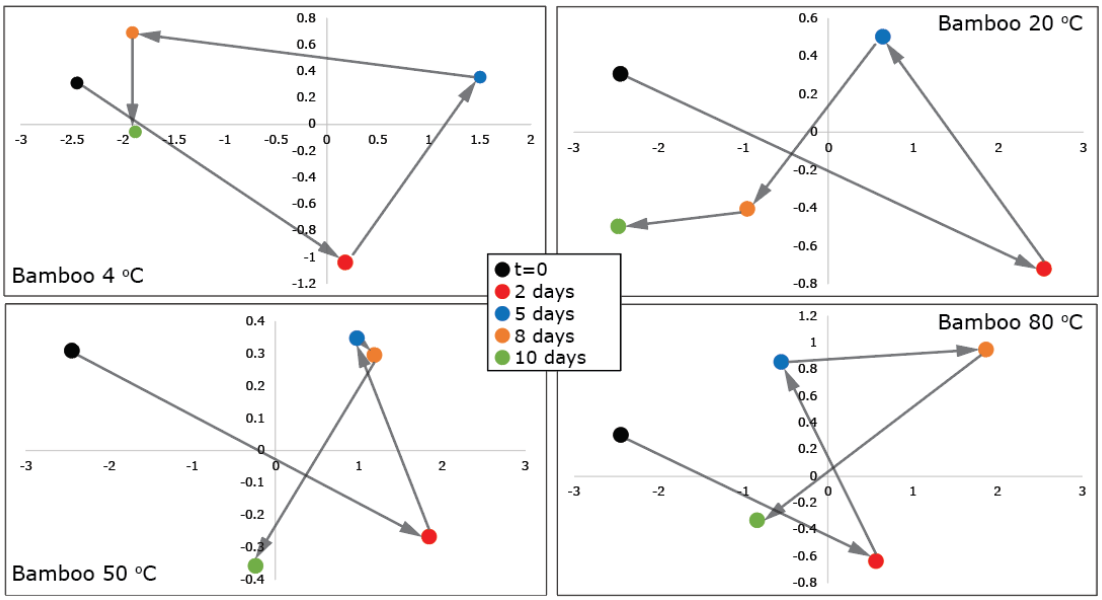

\

Figure 2: A comparison Principle component analysis (PCA) plots bamboo samples cleaned with H_2O_2 and aqua regia at various times of (a) 4 ˚C (b) 20 ˚C (c) 50 ˚C (d) 80 ˚C. Multi-coloured dots represent (Black: t = 0, Red: 2 days, Blue: 5 days, Orange: 8 days, Green: 10 days).